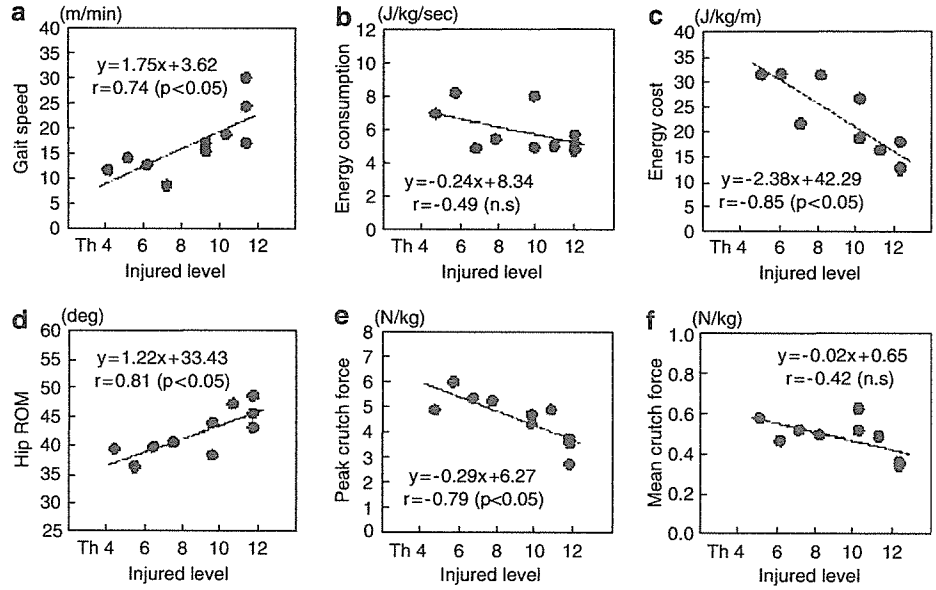

Figure 4 Effects of the level of injury on gait speed, cadence, stride length, energy consumption, energy cost, and hip range of motion. The lines indicate the linear regression lines of the level of injury against each parameter

Table 5 Energy consumption, cost and gait speed with different orthoses in previous studies and our present study

Series	*Number of subjects*	*E. consump (J/kg/s)*	*E. cost (J/kg/m)*	*Gait speed (m/min)*	*Level and aid*
Hirokawa *et al*[5]	6	4.18	21	12.48	T1–T10 RGO
Winchester *et al*[13]	4	4.37	19.44	13.5	T5–T10 RGO
Bernardi *et al*[4]	10	4.3	20	12.78	T4–12 RGO
Felici *et al*[14]	6	8.26	32.3	15.34	T5–L1 RGO, ARGO
Massucci *et al*[15]	6	4.64	29	9.6	T3–T12 ARGO
Ijzerman *et al*[8]	10	5.92	28.20	12.6	T4–12 ARGO
Merati *et al*[16]	6	4.64	24.87	11.2	T3–T11 RGO
Present study	10	6.11	20.12	19.88	T5–12 ARGO
Normal subject					
Blessey[17]		4.35	3.25	82.2	
Bernardi *et al*[18]	18	4.52	3.53	76.8	

All values are expressed as averages

133.0±21.63 b/min, respectively (Table 2), approximately a three-fold increase over the respective resting values. We note that the physiological intensity presumed by these valuables tended to be larger in the higher thoracic SCI subjects. This is clearly shown in Figure 2, where we show that the energy consumption in the higher thoracic SCI subjects is relatively larger, while that in the lower thoracic SCI subjects remained at the same level as that of normal walking. As the subjects were asked to walk at their preferred speed, this result suggests that higher level SCI persons cannot walk comfortably because of their larger area of motor paralysis.

Although the physiological intensity of orthotic gait is in a feasible range to allow safe walking because these patients have sufficient aerobic capacity even in the higher thoracic SCI subjects, the excess energy expenditure and burden on their upper limbs make it impossible to achieve suitable exercise intensity for promoting general health. Therefore, it is important to discover ways to reduce this excess physiological load. In the following section, we will discuss the reason for limited orthotic gait performance in higher thoracic level of SCI patients based on our results of motion analysis.

Relevance between residual motor function and orthotic gait mechanics

During orthotic gait with the ARGO, in order to swing the paralyzed lower limb, the user first puts his or her

weight onto one foot, and rises up the upper body by coincidentally pushing the ground throughout the crutch. By inducing this upper body motion, the reciprocating device mounted on the hip joint functions to swing opposite side of the leg.[7,8] Therefore, the trunk muscle contraction and compensatory upper limb motion are important for creating the hip swing motion. The mechanics of orthotic gait are the key to explaining our results. As clearly shown in Figures 3 and 4d, subjects with higher thoracic injuries showed a remarkably small hip ROM as compared to that in lower thoracic SCI subjects. This result might imply that the upper body motion was insufficient to produce the leg swing in higher level SCI subjects because of their trunk and hip muscle paralysis. Concerning the CF, as is clearly shown in Figure 4e, PCF shows an inverse relationship to the injury level. This result indicates an additional upper limb burden in the compensation for the trunk paralysis in the higher thoracic SCI subjects. It is therefore considered that the slower gait speed and higher energy cost of higher thoracic SCI subjects may be attributed to the limited hip motion and excess upper limb load.

Comparison with previous results

As compared to the other reports[4,5,13–16] where the energy expenditure of orthotic gait was measured in reciprocating gait orthosis (RGO and ARGO), our data shows a faster gait speed with similar energy expenditures (Tables 4 and 5). The gait speed reported by Massucci *et al*[15] and Ijzerman *et al*[8] both of which used ARGO, was remarkably slower than that shown in our data. Taken together with the similarity in the injured level of the subjects between these two studies, this result may indicate that our degree of training especially in time spent practicing, may have influenced the gait speed. Our subjects initially showed a slower gait speed, and reached exhaustion in only a few minutes. However, throughout the training period, they had acquired gait skills and thus improved their energy cost when performing the orthotic gait.

When the present results for energy expenditure during orthotic gait are compared to those for energy expenditure during walking in neurologically normal persons,[17,18] although the levels of energy consumption are within a similar range, the levels of energy cost are considerably worse (approximately six times) during orthotic gait.

Implication for rehabilitation

Owing to the physiological need of gait training for SCI patients, it is important to find a way to reduce the excess physiological load during orthotic gait movement. Many researchers have paid attention to this issue, and in some studies they have attempted to accomplish effective orthotic gait performance with the use of functional electrical stimulation (FES). Although some studies suggested the effectiveness of FES based on the additional muscle contraction of the paralyzed area in, for instance, the reduced energy cost (Hirokawa *et al*[5]), it is obvious that the FES technique is insufficient as a solution to the above problem.

In addition to the higher energy cost of orthotic gait movement, the present results clearly show the relationship between orthotic gait performance and the thoracic level of lesion in SCI patients. Further, the results of the motion analysis have revealed that the slower gait speed and higher energy cost of higher thoracic SCI subjects can be attributed to their limited hip motion and presumed excess upper limb load. Our results indicate that higher thoracic SCI patients need some way of reducing the excess physiological load to acquire the suitable exercise intensity.

References

1 Gordon EE, Vanderwalde H. Energy requirements in paraplegic ambulation. *Arch Phys Med Rehabil* 1956; **37:** 276–285.
2 Chantraine A, Crielaard JM, Onkelinx A, Pirnay F. Energy expenditure of ambulation in paraplegics: effects of long term use of bracing. *Paraplegia* 1984; **22:** 173–181.
3 Nene AV, Patrick JH. Energy cost of paraplegic locomotion with the ORLAU parawalker. *Spinal Cord* 1989; **27:** 5–18.
4 Bernardi M, Canale I, Castellano V, Di Filippo L, Felici F, Marchetti M. The efficiency of walking of paraplegic patients using a reciprocating gait orthosis. *Paraplegia* 1995; **33:** 409–415.
5 Hirokawa S, Grimm M, Le T, Solomonow M, Baratta RV, D'Ambrosia RD. Energy consumption in paraplegic ambulation using the reciprocating gait orthosis and electric stimulation on the thigh muscles. *Arch Phys Med Rehabil* 1990; **71:** 687–694.
6 Butler PB, Major RE, Patrick JH. The technique of reciprocal walking using the hip guidance orthosis (hgo) with crutches. *Prosthet Orthot Int* 1984; **8:** 33–38.
7 Jefferson RJ, Whittle MW. Performance of three walking orthoses for the paralysed: a case study using gait analysis. *Prosthet Orthot Int* 1990; **14:** 103–110.
8 IJzerman MJ, Baardman G, van 't Hof MA, Boom HB, Hermens HJ, Veltink PH. Validity and reproducibility of crutch force and heart rate measurements to assess energy expenditure of paraplegic gait. *Arch Phys Med Rehabil* 1999; **80:** 1017–1023.
9 Solomonow M, Baratta RV, D'Ambrosia R. Standing and walking after spinal cord injury: experience with the reciprocating gait orthosis powered by electrical muscle stimulation. *Top Spinal Cord Injury Rehabil* 2000; **5:** 29–53.
10 Kawashima N, Nakazawa K, Ishii N, Akai M, Yano H. Potential impact of orthotic gait on natural killer cell activities in thoracic level of spinal cord injured patients. *Spinal Cord* 2004; **42:** 420–424.
11 Maynard Jr FM *et al.* International standards for neurological and functional classification of spinal cord injury. *Spinal Cord* 1997; **35:** 266–274.
12 Nene AV, Patrick JH. Energy cost of paraplegic locomotion using the parawalker-electrical stimulation 'hybrid' orthosis. *Arch Phys Med Rehabil* 1990; **71:** 116–120.

13 Winchester PK *et al.* A comparison of paraplegic gait performance using two types of reciprocating gait orthoses. *Prosthet Orthot Int* 1993; **17:** 101–106.
14 Felici F, Bernardi M, Radio A, Marchettoni P, Castellano V, Macaluso A. Rehabilitation of walking for paraplegic patients by means of a treadmill. *Spinal cord* 1997; **35:** 383–385.
15 Massucci M, Brunetti G, Piperno R, Betti L, Franceschini M. Walking with the advanced reciprocating gait orthosis (ARGO) in thoracic paraplegic patients: energy expenditure and cardiorespiratory performance. *Spinal cord* 1998; **36:** 223–227.
16 Merati G, Sarchi P, Ferrarin M, Pedotti A, Veicsteinas A. Paraplegic adaptation to assisted-walking: energy expenditure during wheelchair *versus* orthosis use. *Spinal Cord* 2000; **38:** 37–44.
17 Blessey R. Energy cost of normal walking. *Orthop Clin North Am* 1978; **9:** 356–358.
18 Bernardi M *et al.* Cost of walking and locomotor impairment. *J Electromyogr Kinesiol* 1999; **9:** 149–157.

Spinal Cord (2006) 44, 522

www.nature.com/sc

Erratum

Effect of lesion level on the orthotic gait performance in individuals with complete paraplegia

N Kawashima, D Taguchi, K Nakazawa and M Akai

Spinal Cord (2006) **44**, 522. doi:10.1038/sj.sc.3101941

Correction to: *Spinal Cord* (2006) **44**, 487–494. doi:10.1038/sj.sc.3101916; published online 21 March 2006

Owing to a typesetting error, Figure 4 in the above paper was published inaccurately. A corrected figure is shown below.

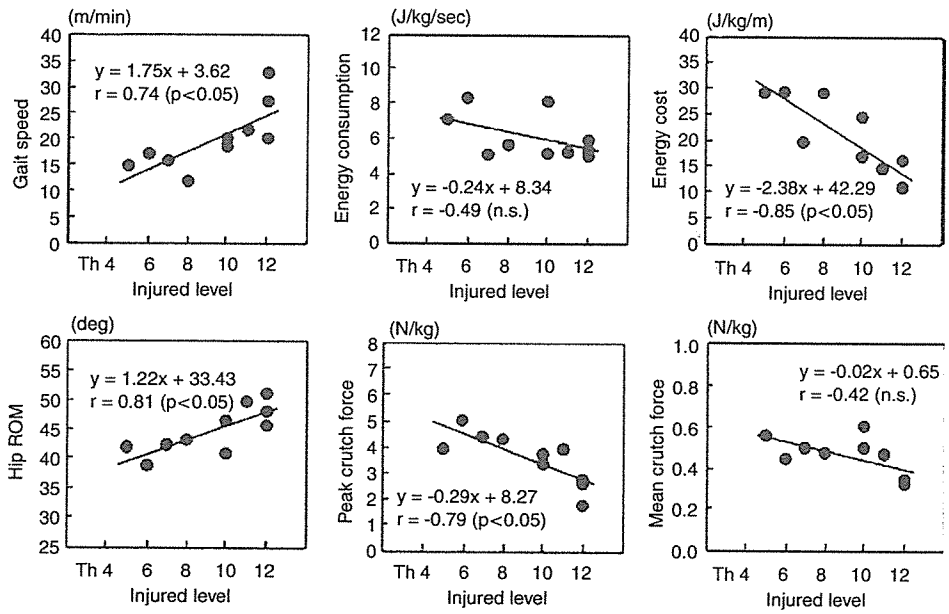

Figure 4 Effects of the level of injury on gait speed, cadence, stride length, energy consumption, energy cost, and hip range of motion. The lines indicate the linear regression lines of the level of injury against each parameter

Spinal Cord (2006) 44, 480–486

www.nature.com/sc

Original Article

Cardiorespiratory responses during passive walking-like exercise in quadriplegics

Y Higuchi*[,1], S Kitamura[1], N Kawashima[2], K Nakazawa[2], T Iwaya[3] and M Yamasaki[4]

[1]*Department of Physical Training for Remedial Gymnastics, Hospital, National Rehabilitation Center for Persons with Disabilities, Tokorozawa, Saitama, Japan;* [2]*Department of Rehabilitation for the Movement Functions, Research Institute of the National Rehabilitation Center for Persons with Disabilities, Tokorozawa, Saitama, Japan;* [3]*Rehabilitation training center, National Rehabilitation Center for Persons with Disabilities, Tokorozawa, Saitama, Japan;* [4]*Department of Health Science, Faculty of Integrated Arts and Sciences, Hiroshima University, Japan*

Study design: Cross-sectional and comparative investigation using quadriplegics (QP) and nondisabled subjects (ND).
Objective: To evaluate cardiorespiratory responses during passive walking-like exercise (PWE) in QP.
Setting: National Rehabilitation Center for Persons with Disabilities in Japan.
Method: The subjects were seven male QP with complete lesion (age: 27.0±5.4, injured level: C6–C7) and six male ND (age: 26.3±4.5). Cardiorespiratory responses were measured until voluntary fatigue during PWE, the rhythmical activity of paralyzed lower limbs synchronized with arm movements.
Results: There were no significant differences in oxygen consumption ($\dot{V}O_2$), pulmonary ventilation ($\dot{V}E$), heart rate (HR) and oxygen pulse (O_2 pulse) between QP and ND during PWE. ND showed increased ventilatory equivalent for oxygen ($\dot{V}E/\dot{V}O_2$ ratio) during exercise, while QP showed a significantly greater respiratory rate (RR) during exercise than ND ($P<0.05$).
Conclusion: PWE elicited an increase in $\dot{V}O_2$ with workload increment in QP similar to ND. However, higher RR suggested the intrinsic dysfunction of RR control during submaximal exercise in QP. From these results, it was thought that respiratory response would be the restriction factor of efficient oxygen transportation during PWE in QP.
Spinal Cord (2006) **44**, 480–486. doi:10.1038/sj.sc.3101875; published online 29 November 2005

Keywords: quadriplegics; passive walking-like exercise; cardiorespiratory response

Introduction

For individuals with spinal cord injury (ISCI), it is difficult to improve their cardiorespiratory function and to activate the oxygen supply function by exercise training such as wheelchair or arm swinging exercise because of the characteristics of the obstacles.[1,2] In general, the peak oxygen uptake (peak $\dot{V}O_2$) is dependent on the level of spinal cord injury (SCI), and quadriplegics (QP) and high lesion paraplegics (PP) show a lower peak $\dot{V}O_2$ than nondisabled (ND) or low lesion PP.[3–5] In addition, during submaximal exercise, QP and high lesion PP showed the reduced ventilation efficiency, stroke volume, venous return and sympathetic activity in comparison to ND or low lesion PP.[5,6]

For such ISCI with low physiological responses to exercise, the exercise posture is an important factor enhancing the effect of aerobic training. McLean *et al*[7] investigated the influence of body posture in training on aerobic capacity in ISCI and indicated that although improvements in aerobic capacity could be achieved by training in either a supine or a sitting posture, the supine posture had more effect on aerobic training than the sitting posture. One reason is that the supine posture is advantageous to ISCI circulation, because there is small amount of blood in the paralyzed leg compared to the sitting posture due to the lower effect of gravity.

In contrast, in a sitting posture during exercise, venous blood pools in the legs and abdomen, causing reduced filling pressure and diminished ventricular volume. Therefore, when QP and PP perform exercise in a sitting posture, blood is not efficiently redistributed

*Correspondence: Y Higuchi, National Rehabilitation Center for Persons with Disabilities, 4-1 Namiki, Tokorozawa, Saitama 359-8555, Japan

to the working muscles.[8–11] To improve venous blood pooling during exercise in a sitting posture, some researchers have investigated the effect of passive leg exercise on circulation.[9,12] This exercise passively moves the paralyzed lower limbs, the blood stored in lower limbs returns to the heart, and stroke volume increases conjointly with the law of Frank-starling.[9,12]

It is reported that functional electrical stimulation (FES) is also a useful method to decrease venous blood pooling in the legs, because FES increases the activity of muscle pumping and vasoconstriction in the legs.[13–15] Bhambhani *et al*[16] measured the deoxygenation of the quadriceps muscle during FES using QP and PP. They indicated that the muscle deoxygenation of paralyzed muscles occurred more quickly with metabolic responses in the paralyzed muscles. Mutton *et al*[17] reported a significant increase in peak $\dot{V}O_2$ during hybrid exercise[18–20] that combined upper arm exercise with FES in QP and PP when compared with only FES. Moreover, Raymond *et al*[18] showed a higher oxygen intake and lower heart rate (HR) during hybrid exercise including arm-swinging exercise at a workload of 65% maximal oxygen uptake in PP. In addition, Hooker *et al*[21] compared the respiratory and circulatory responses during hybrid exercise with those during submaximal arm-swinging exercise and FES leg-cycle exercise in QP. They showed higher pulmonary ventilation ($\dot{V}E$), oxygen uptake ($\dot{V}O_2$) and carbon dioxide elimination during hybrid exercise than the other two exercises, but a higher stroke volume than only arm-swinging exercise. They concluded that hybrid exercise using whole-body exercise, including the paralyzed muscles, is effective in improving the cardiorespiratory function of ISCI.

More recently, it has been reported that standing gait exercise with orthoses has a good influence on cardiorespiratory function in ISCI.[22] Faghri *et al*[13,23] investigated the physiological reaction of a standing posture on ISCI with and without FES. They showed stable cardiac output, stroke volume and total peripheral resistance (TPR) during 30 min standing with FES in both QP and PP. In contrast, during passive standing without FES, QP demonstrated significantly higher TPR and significantly lower systolic blood pressure and mean arterial pressure than PP. Faghri *et al*[13,23] also indicated that standing without FES was disadvantageous to the regulation of hemodynamics during posture change in QP.

When ISCI passively walked on a treadmill using body weight support equipment, they showed a similar electromyographic pattern in the paralyzed muscles to ND.[24] Furthermore, Colombo *et al*[25] obtained the same result during passive stepping using driven gait orthosis for C3 (incomplete) and C5 (complete). It is naturally expected that passive walking with arm exercise increases energy expenditure and oxygen supply to the arm is elevated. However, as far as we know, there are no studies investigating the cardiorespiratory responses of QP during passive walking-like exercise (PWE) when standing.

The purpose of this study, therefore, was to clarify respiratory and circuratory responses during PWE by a stepwise incremental method and to compare the results of QP with those of ND.

Methods

Subjects

Seven male patients with complete chronic QP and six ND male subjects volunteered to participate in this study. Table 1 lists their physical characteristics. The lesion in SCI was located between C6 and C7. All subjects regularly performed wheelchair sports, such as twin basketball, quad rugby and distance running, for more than 60 min a day and more than twice a week. No subject had a history of cardiovascular, metabolic, or pulmonary disease. Informed consent was obtained from all subjects before their participation in this study. The subject refrained from food, caffeine and nicotine for at least 3 h before testing. The study was approved by the Ethical Research Committee in the National Rehabilitation Center for Persons with Disabilities.

Testing protocols

All subjects performed an incremental exercise test on an Easy Stand Glider 6000 (Altimate Medical Int.,

Table 1 Characteristics of the subjects

No	*Sex*	*Height (cm)*	*Weight (kg)*	*Age (years)*	*Level of injury*	*Zancolli*	*ASIA*	*Times of injury (month)*	*Sports*
a	M	163.0	57.3	34	C6	2B3	A	153	Twin basketball
b	M	168.0	55.7	23	C6	2B1	A	32	Twin basketball
c	M	174.0	55.1	29	C6	2B2	A	27	Twin basketball
d	M	166.0	52.3	29	C6	2B1	A	81	Distance running
e	M	160.0	41.3	20	C7	3A	A	25	Twin basketball
f	M	177.0	69.8	22	C7	3A	B	54	Quad rugby
g	M	172.0	66.6	32	C6	2B1	A	107	Quad rugby
h	M	168.0	59.7	25	ND				Track and field
i	M	180.0	62.2	26	ND				Soccer
j	M	172.0	62.5	35	ND				Track and field
k	M	175.0	68.4	23	ND				Track and field
l	M	168.0	65.0	26	ND				Baseball
m	M	170.0	54.0	23	ND				Skiing

Morton, MN, USA). The Easy Stand Glider 6000 is designed to strengthen both the upper and lower extremities while standing. It has a safety belt around the waist, a chest pad, hip guide and knee support. When the subject swings his arms back and forth, his legs simultaneously move passively just like walking. Tests were performed with the push and pull handle horizontal to the level of the shoulder joint and elbows slightly flexed at the point of maximal arm extension (Figure 1).

The subjects remained seated in a wheelchair or chair for at least 30 min. Baseline physiological measurements were recorded for the last 5 min during seating. They were subsequently guided with a metronome for reciprocal movement of the arms and legs while standing. Exercise commenced by swinging the arms back and forth at 20 times/min for 2 min. The swings were then increased to 10 times/min every 2 min until 50 times/min, and then 5 times/min every 2 min until exhaustion. The incremental exercise test was terminated when voluntary fatigue was attained. Voluntary fatigue was defined as the point at which the subject could no longer keep pace and his RPE was over 15. The experiment was carried out in a room with ambient temperature and relative humidity maintained at 22–25°C and 30–50%, respectively.

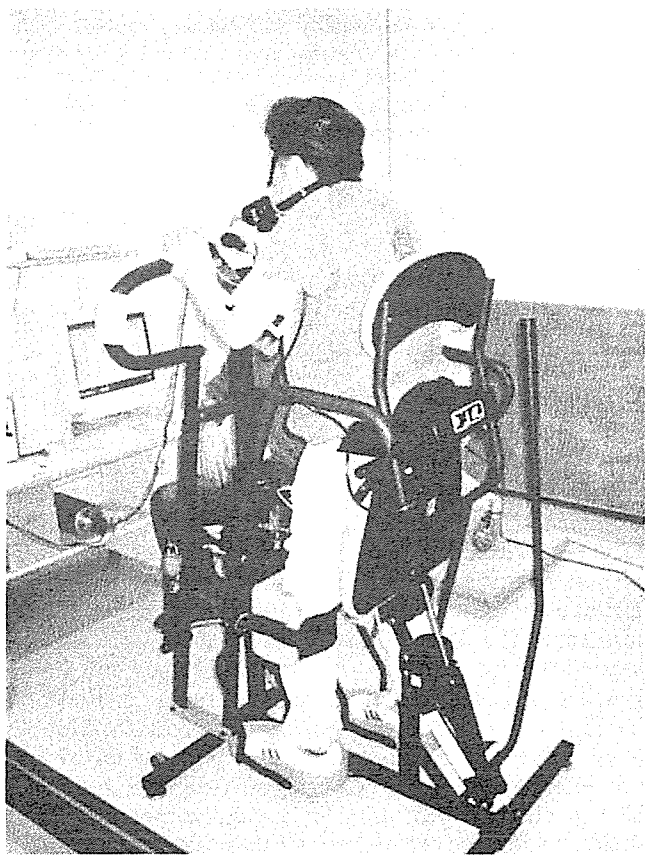

Figure 1 The arm swinging and passive walking machine. When a quadriplegic subject swings his arms back and forth, the paralyzed legs simultaneously move as if walking

Cardiorespiratory measurements

Cardiorespiratory measurements were continuously monitored during the test using the gas analyzer of the metabolic system (Model AT-3000, Anima, Tokyo, Japan). The gas analyzer was calibrated using standard gas concentrations (16.1% oxygen, 5.01% carbon dioxide). The volume transducer was calibrated using a syringe calibrated to 2 l. The gas analyzer was programmed to present the following results: absolute $\dot{V}O_2$ (l/min), relative $\dot{V}O_2$ (ml/kg/min), respiratory rate (RR, times/min) and $\dot{V}E$ (l/min). The following variables were calculated from the oxygen pulse (O_2 pulse, ml/beat) as the ratio between absolute $\dot{V}O_2$ and HR (beats/min), and the ventilatory equivalent for oxygen ($\dot{V}E/\dot{V}O_2$ ratio, l/ml) as the ratio between $\dot{V}E$ and absolute $\dot{V}O_2$.

HR was recorded during the last 10 s at each work stage using a wireless monitor (Life Scope 8/Two, Nihon Koden, Tokyo, Japan). Blood was sampled from the earlobe during rest and exercise and blood lactate accumulation (LA, mmol/ml) was measured using a simplified blood lactate test meter (Lactate Pro™ LT-1710, Arckly, Inc., Kyoto, Japan). Blood sampling was conducted immediately after rest and within 30 s after each workload. The sampling time was within 20 s.

Statistical analysis

All variables were expressed as the mean ± SD. Two-way repeated analysis of variance was used to compare the difference between groups. *P*-values <0.05 were considered significant.

Results

Figure 2a shows the relationship between $\dot{V}O_2$ and workload in QP and ND. $\dot{V}O_2$ within the workload of 60 times/min varied little and almost no rise was observed. At a workload of 65 times/min, $\dot{V}O_2$ started to increase rapidly. At any workload, there was no significant difference between the groups. Changes in $\dot{V}E$ and LA over time during exercise were similar to those in $\dot{V}O_2$. No significant differences were found in $\dot{V}E$ and LA between QP and ND.

HR increased with the workload increment in both groups (Figure 2b). When the workloads were between 40 and 70 times/min, there was little increase in HR for QP and ND. Although QP showed a higher HR than ND during rest and exercise, significant difference was only found at a workload of 30 times/min. Figure 2c indicates the O_2 pulse over the time course of exercise. In ND, the O_2 pulse remained unchanged from the beginning of exercise to a workload of 60 times/min. Subsequently, the O_2 pulse of QP increased rapidly. In contrast, QP showed a gradual increase in the O_2 pulse linearly with the workload. The O_2 pulse of QP was higher than that of ND at any workload and significant difference was only found at the beginning of exercise (20 times/min).

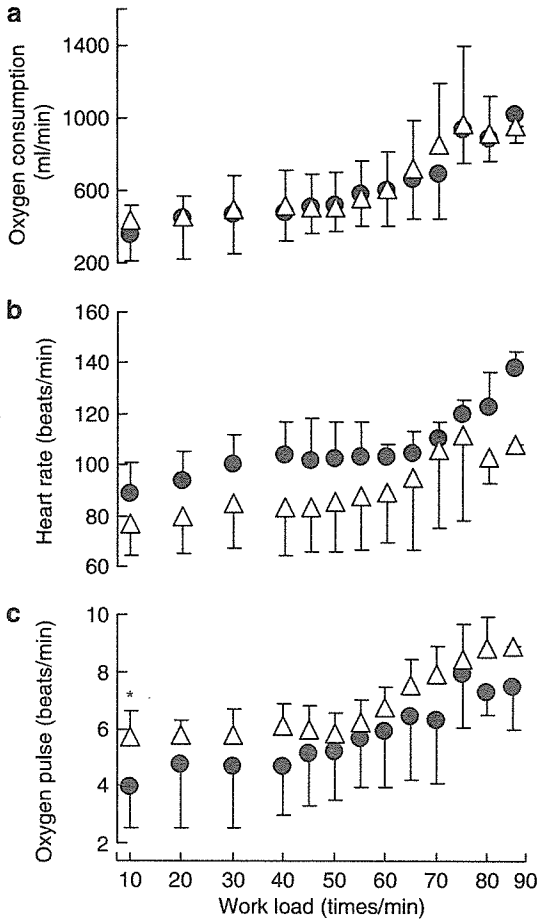

Figure 2 Change in oxygen consumption (**a**), heart rate (**b**), and oxygen pulse (**c**) during passive walking with arm swinging exercise in persons with Quadriplegics (●) and nondisabled (△). Although there was no difference of oxygen consumption between QP and ND, oxygen transportation of QP was inferior to ND during the exercise. $^{*}P<0.05$: compared with nondisabled subjects

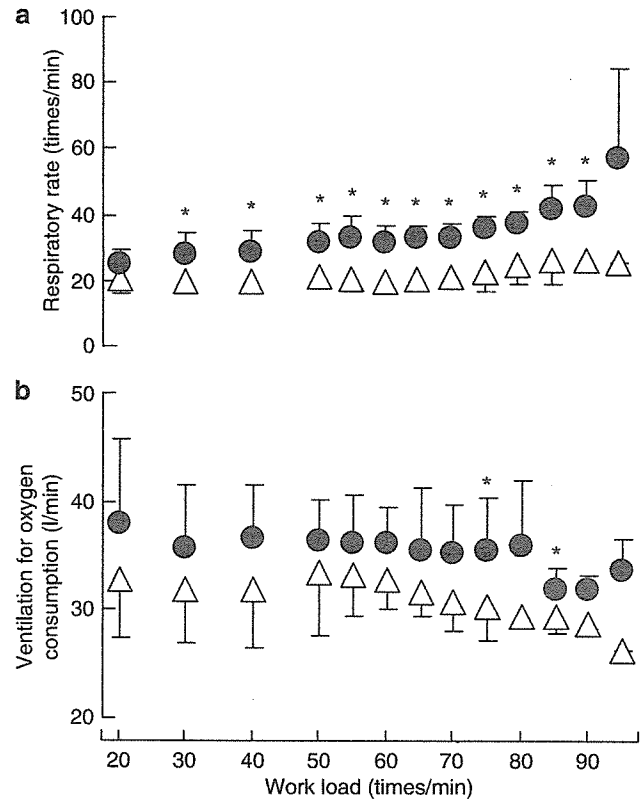

Figure 3 Change in respiratory rate (**a**) and ventilation for oxygen consumption (**b**) during passive walking with arm swinging exercise in persons with Quadriplegics (●) and nondisabled (△). Ventilation efficiency showed significant decrease in QP as compared with ND. $^{*}P<0.05$, $^{\#}P<0.01$: compared with nondisabled subjects

Figure 4a illustrates the relationship of HR to $\dot{V}O_2$ in QP and ND. With increasing $\dot{V}O_2$, HR linearly and significantly increased in both groups. When $\dot{V}O_2$ was around 500 ml, HR of QP was apparently greater than ND.

There existed a great difference in RR between QP and ND during exercise (Figure 3a). ND had almost unchanged RR during exercise. In contrast to ND, QP showed increased RR over the time course of exercise. There were significant differences in RR between the groups at any workload except the lowest (20 times/min) and the highest (95 times/min). Figure 3b shows the $\dot{V}E/\dot{V}O_2$ ratio during the incremental exercise test in QP and ND. The $\dot{V}E/\dot{V}O_2$ ratio of QP was higher than that of ND at any workload and significant differences were found at higher workloads of 75 and 85 times/min.

The relationship of RR to $\dot{V}E$ is illustrated in Figure 4b with regression lines. The regression line of QP shifted to the upper side of ND, indicating that QP required more RR to achieve the same $\dot{V}E$ as ND.

Discussion

In this study, there were no significant differences in $\dot{V}O_2$ and $\dot{V}E$ during standing exercise between QP and ND (Figure 2a). Some investigators showed that the cardiorespiratory responses of QP during arm exercise were relatively lower than ND and PP,[4,5,26] suggesting that the cardiorespiratory responses of ISCI are largely dependent on the level of SCI.[3,6,27] These results were obtained from arm-swinging exercise or wheelchair ergometer exercise requiring mainly upper limb activity in a sitting posture. It may be considered that the exercise while sitting, using only the upper limbs, influences the $\dot{V}O_2$ of ISCI. Hopman *et al*[28] demonstrated that peak $\dot{V}O_2$ significantly increased in a supine posture during maximal arm-swinging exercise in comparison with a sitting posture. In addition, McLean *et al*[7] compared the power output (PO) of QP during an intermittent progressive peak exercise test in a sitting posture with that in a supine posture. As a result, they reported higher PO in a sitting than supine posture. These investigations suggest that cardiorespiratory responses during exercise are affected by exercise postures in QP.

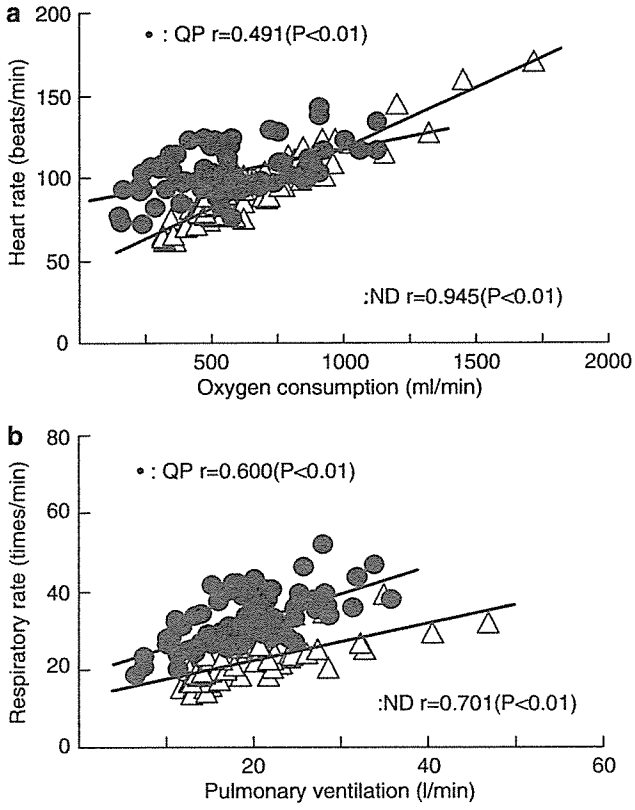

Figure 4 Relationship between oxygen consumption and heart rate (**a**), pulmonary ventilation and respiratory rate (**b**) during passive walking in persons with Quadriplegics (●) and nondisabled (△). QP showed inactive to HR and remarkable increase in RR as compared with ND

Cardiorespiratory responses during exercise in QP change with passive exercise by the paralyzed limbs in addition to the exercise posture. Pitetti *et al*[29] carried out arm-swinging exercise in ISCI and ND with lower body positive pressure (LBPP). They found a significant increase in $\dot{V}O_2$, $\dot{V}E$ and work rate during arm-swinging exercise with LBPP compared to without LBPP. Furthermore, there were no differences in $\dot{V}O_2$, $\dot{V}E$ and work rate between ISCI and ND during exercise with LBPP. From these results, Pitetti *et al*[29] suggested that for ISCI, LBPP augmented the exercise capacity by preventing the redistribution of blood to the lower extremities. Hopman *et al*[27,28] investigated the effects of exercise posture, wearing an antigravity suit (anti-G suit), elastic stocking and abdominal binder, and FES on blood redistribution and circulatory responses in QP and PP. They demonstrated that $\dot{V}O_2$ and HR decreased by wearing an anti-G suit and increased by FES, and increased by wearing elastic stockings and FES during submaximal exercise. In contrast, during maximal exercise, only FES increased $\dot{V}O_2$ and HR. From these results, Hopman *et al*[27,28] suggested that these methods of circulatory redistribution have different working mechanisms and the effects are dependent on the SCI level probably because of differences in active muscle mass, sympathetic impairment and blood pressure values. Furthermore, $\dot{V}O_2$ increased significantly during FES exercise of lower limbs in comparison with at rest[30] and $\dot{V}O_2$ during hybrid exercise was higher than that during arm-swinging exercise or leg cycle exercise by FES.[17,21,31]

The findings using the passive activity of paralyzed lower limbs and FES in addition to arm exercise clearly demonstrated good effects on cardiorespiratory responses and improving the efficiency of their oxygen utilization in ISCI. However, these studies were mostly performed in a sitting posture. If ISCI perform exercise in a standing posture, the cardiorespiratory responses may be different from those in a sitting posture. Nash *et al*[32] showed significant increases in $\dot{V}O_2$, $\dot{V}E$ and HR during PWE when standing by using lobotic-assisted locomotion in QP with a lesion level of C3–C4. In addition, Dietz *et al*[24] identified electromyographic activities of the musculus tibialis anterior and musculus soleus during passive walking on a treadmill in QP and PP. These investigations suggested that PWE in a standing posture with arm exercise in QP facilitated cardiorespiratory responses. Our study showed the same $\dot{V}O_2$ between QP and ND, indicating that the rhythmical activity of paralyzed limb increased $\dot{V}O_2$.

In the present study, QP showed a significantly higher RR from 30 to 90 times/min (Figure 3b), and QP increased RR to the equivalent $\dot{V}E$ of the ND (Figure 4b). Coutts *et al*[6] found lower respiratory parameters such as $\dot{V}E$ and ventilation equivalent in QP than in PP during submaximal arm-swinging exercise. The ventilation equivalent is generally considered to be a measure of breathing efficiency, and decreases during submaximal exercise are associated with increased tidal volume and relative decreases in dead space ventilation.[6] Bhambhani *et al*[16] demonstrated that the $\dot{V}E/\dot{V}O_2$ ratio in ISCI, including QP, is lower during FES cycle exercise than ND, indicating that the ventilatory efficiency of ISCI is inferior to that of ND. In good agreement with the data of Bhambhani *et al*,[16] we found a lower $\dot{V}E/\dot{V}O_2$ ratio of QP in comparison with ND. There was no difference in LA between QP (2.9 ± 1.1 mmol/l) and ND (3.0 ± 1.6 mmol/l) during peak exercise, indicating that the increase in RR was not related to metabolic factors, because LA stimulates the respiratory center and consequently increases the elimination of carbon dioxide. Furthermore, it has been reported that expiratory muscle contraction is influenced by sympathetic nerve activity more than muscle metaboreflex.[33]

In AB, the impulse from the motor area of the cerebral cortex via the center of breathing adjusts the ventilation equivalent to the exercise intensity during exercise.[34] In addition, it has been demonstrated that respiration is regulated by transmitting the afferent information from activity muscles to the center.[35] In QP, the afferent information from the agonist of the upper limbs was transmitted to the center during exercise; however, the nerve impulse of the ventilatory regulation corresponding to the workload is not sent to the

respiratory muscles. That is, it is believed that the afferent information to the center increased excessively in our tests. Restrictive ventilatory impairment may disturb respiratory regulation during exercise in QP.

Green[36] found that excitations of the stretch receptors stimulated by the stretch reflex (the Hering–Breuer reflex) in the lung were relayed via the vagus nerve to the medullary respiratory center, leading to a reflex decrease in tidal volume. This reflex was not found in normal adults and in babies with undeveloped respiratory-related muscles and in some animals.[36]

We hypothesized that QP with restrictive ventilatory impairment might show a condition similar to that of the babies in Green's study. To compensate for the decrease in tidal volume by the Hering–Breuer reflex and to achieve the same ventilation as ND, QP increased RR from the commencement of exercise. Specifically, the increase in RR in QP could be a result of the increased afferent information from the agonist to the respiratory center and the increased reflex induced by restrictive ventilatory impairment.

Some investigators have shown a lower maximal HR below 110 beats/min in QP than that of PP and ND.[4,37] Bhambhani *et al*[16] found no significant difference of HR in ISCI including QP during FES exercise from that at rest. A lower HR during exercise is naturally expected in QP because of sympathetic activity dysfunction controlling the heart. In this study, however, during peak exercise, the HR of QP was higher than the data of Bhambhani *et al*,[16] and there were no significant differences of HR between QP and ND similar to $\dot{V}O_2$ (Figure 2b). Muraki *et al*[12] reported a significant increase in stroke volume and cardiac output without a rise of HR during passive leg cycle exercise in PP. They suggested the promotion of venous return related to the lengthening and shortening of the paralyzed muscle without tension in the lower limbs.

In this study, HR in QP increased during PWE. This is not consistent with the findings of Faghri *et al*,[23] who found no increase of HR in QP during FES when standing. On the other hand, they reported increased TPR, which could be a compensatory mechanism to control the significant drop in blood pressure occurring during standing in QP. Hooker *et al*[21] investigated cardiorespiratory responses during arm-swinging exercise, FES leg-cycle exercise and hybrid exercise in QP, and revealed that $\dot{V}O_2$, $\dot{V}E$ and HR were higher during hybrid exercise than the other two exercises and there was no significant difference in stroke volume between the hybrid exercise and FES leg-cycle exercise. Dela *et al*[14] reported that although HR increased immediately after the commencement of FES and attained a steady state in ND, QP showed a delay in the HR increment. HR responses in QP may be attributable to arterial baroreceptors that elevate HR in QP with the lower blood pressure developed during exercise.[14]

In this study, there was no significant difference in HR between QP and ND during peak passive walking. On the other hand, during submaximal exercise, a clear difference in HR was found between QP and ND. In ND, HR increased linearly with workload increment, while it increased in QP from the commencement of exercise to 40 times/min and HR increased gradually, showed a steady state between 50 and 75 times/min, increasing remarkably after 80 times/min (Figure 2b). It could be expected that HR in QP increased by the activation of arterial baroreceptors in compensation for deficient blood distribution from the beginning of exercise to 40 times/min, while between 50 and 75 times/min, HR showed a steady state because blood was distributed sufficiently to agonists (Figure 2c).

In conclusion, PWE, the rhythmical activity of paralyzed lower limbs synchronized with arm movements, elicited an increase in $\dot{V}O_2$ in QP similar to ND. However, higher RR suggested the intrinsic dysfunction of RR control during submaximal exercise in QP. From these results, it was thought that respiratory responses would restrict the efficiency of oxygen transportation during PWE in QP.

References

1 Hjeltnes N, Wallberg-Henriksson H. Improved work capacity but unchanged peak oxygen uptake during primary rehabilitation in tetraplegic patients. *Spinal Cord* 1998; **36:** 691–698.
2 Birk TJ, Nieshoff E, Gray G, Steeby J, Jablonski K. Metabolic and cardiopulmonary responses to acute progressive resistive exercise in a person with C4 spinal cord injury. *Spinal Cord* 2001; **39:** 336–339.
3 Bernard PL, Mercier J, Varry A, Prefaut C. Influence of lesion level on the cardioventilatory adaptations in paraplegic wheelchair athletes during muscular exercise. *Spinal Cord* 2000; **38:** 16–25.
4 Coutts KD, Rhodes EC, McKenzie DC. Maximal exercise responses of tetraplegics and paraplegics. *J Appl Physiol* 1983; **55:** 479–482.
5 Schimid A *et al.* Catecholamines, heart rate, and oxygen uptake during exercise in persons with spinal cord injury. *J Appl Physiol* 1998; **85:** 635–641.
6 Coutts KD, Rhodes EC, McKenzie DC. Submaximal exercise responses of tetraplegics and pareplegics. *J Appl Physiol* 1985; **59:** 237–241.
7 McLean KP, Skinner JS. Effect of body training position on outcomes of an aerobic training study on individuals with quadriplegia. *Arch Phys Med Rehabil* 1995; **76:** 139–150.
8 Davis GM. Exercise capacity of individuals with paraplegia. *Med Sci Sports Exerc* 1993; **25:** 423–432.
9 Hopman MT. Circulatory responses during arm exercise in individuals with paraplegia. *Int J Sports Med* 1994; **15:** 126–131.
10 Mathias CJ, Frankel HL. Cardiovascular control in spinal man. *Ann Rev Physiol* 1988; **50:** 577–592.
11 Olive JL, Mccully KK, Dudley GA. Blood flow response in individuals with incomplete spinal cord injuries. *Spinal Cord* 2002; **40:** 639–645.
12 Muraki S, Yamasaki M, Ehara Y, Kikuchi K, Seki K. Cardiovascular and respiratory responses to passive leg cycle exercise in people with spinal cord injuries. *Eur J Appl Physiol* 1996; **74:** 23–28.
13 Faghri PD, Yount J. Electrically induced and voluntary activation of physiologic muscle pump: a comparison

between spinal cord-injured and able-bodied individuals. *Clin Rehabil* 2002; **16:** 878–885.
14 Dela F *et al.* Cardiovascular control during exercise insights from spinal cord-injury humans. *Circulation* 2003; **107:** 2127–2133.
15 Kjaer M, Pott F, Mohr T, Linkis P, Tornoe P, Secher NH. Heart rate during exercise with leg vascular occlusion in spinal cord-injured humans. *J Appl Physiol* 1999; **86:** 806–811.
16 Bhambhani Y, Tuchak C, Burnham R, Jeon J, Maikala R. Quadriceps muscle deoxygenation during functional electrical stimulation in adults with spinal cord injury. *Spinal Cord* 2000; **38:** 630–638.
17 Mutton DL, Scremin AME, Barstow TJ, Scott MD, Kunkel CF, Cable TG. Physiologic responses during functional electrical stimulation leg cycle and hybrid exercise in spinal cord injured subjects. *Arch Phys Med Rehabil* 1997; **78:** 712–718.
18 Raymond J, Davis GM, Fahey A, Climstein M, Sutton JR. Oxygen uptake and heart rate responses during arm versus combined arm + ES-induced leg exercise in people with paraplegia. *Spinal Cord* 1997; **35:** 680–685.
19 Laskin JJ *et al.* Electrical stimulation-assisted rowing exercise in spinal cord injured people. A pilot study. *Paraplegia* 1993; **31:** 534–541.
20 Wheeler GD *et al.* Functional electric stimulation-assisted rowing: increasing cardiovascular fitness through functional electric stimulation rowing training in persons with spinal cord injury. *Arch Phys Med Rehabil* 2002; **83:** 1093–1099.
21 Hooker SP *et al.* Metabolic and hemodynamic responses to concurrent voluntary arm crank and electrical stimulation leg cycle exercise in quadriplegics. *J Rehabil Res Dev* 1992; **29:** 1–11.
22 Kawashima N, Sone Y, Nakazawa K, Akai M, Yano H. Energy expenditure during walking with weight-bearing control (WBC) orthosis in thoracic level of paraplegic patients. *Spinal Cord* 2003; **41:** 506–510.
23 Faghri PD, Yount JP, Pesce WJ, Seetharama S, Votto JJ. Circulatory hypokinesis and functional electric stimulation during standing in persons with spinal cord injury. *Arch Phys Med Rehabil.* 2001; **82:** 1587–1595.
24 Dietz V, Nakazawa K, Wirz M, Erni T. Level of spinal cord lesion determines locomotor activity in spinal man. *Exp Brain Res* 1999; **128:** 405–409.
25 Colombo G, Wirz M, Dietz V. Driven gait orthosis for improvement of locomotor training in paraplegic patients. *Spinal Cord* 2001; **39:** 252–255.
26 Irizawa M, Yamasaki M, Muraki S, Komura T, Seki K, Kikuchi K. Relationship between heart rate and oxygen uptake during submaximal arm cranking in paraplegics and quadriplegics. *Ann Physiol Anthropol* 1994; **13:** 275–280.
27 Hopman MT, Monroe M, Dueck C, Phillips WT, Skinner JS. Limits to maximal performance in individuals with spinal cord injury. *Int J Sports Med* 1998; **19:** 98–103.
28 Hopman MT, Monroe M, Dueck C, Phillips WT, Skinner JS. Blood redistribution and circulatory responses to submaximal arm exercise in persons with spinal cord injury. *Scand J Rehabil Med* 1998; **30:** 167–174.
29 Pitetti KH, Barrett PJ, Campbell KD, Malzahn DE. The effect of lower body positive pressure on the exercise capacity of individuals with spinal cord injury. *Med Sci Sports Exerc* 1994; **24:** 463–468.
30 Figoni SF *et al.* Physiologic responses of paraplegics and quadriplegics to passive and active leg cycle ergometry. *J Am Paraplegia Soc* 1990; **13:** 33–39.
31 Raymond J, Davis GM, Climstein M, Sutton JR. Cardiorespiratory responses to arm cranking and electrical stimulation leg cycling in people with paraplegia. *Med Sci Sports Exerc* 1999; **31:** 822–828.
32 Nash MS, Jacobs PL, Johnson BM, Field-Fote' E. Metabolic and cardiac responses to robotic-assisted locomotion in motor-complete tetraplegia: a case report. *J Spinal Med* 2004; **27:** 78–82.
33 Derchak PA, Shell AW, Morgan BJ, Dempsey JA. Effects of expiratory muscle work on muscle sympathetic nerve activity. *J Appl Physiol* 2002; **92:** 1539–1552.
34 Krough A, Lindhard J. The reguration of respiration and circulation during the initial stages of muscular work. *J Physiol* 1913; **47:** 112–136.
35 Morikawa T *et al.* Afferent and cardiodynamic drives in the early phase of exercise hyperpnea in humans. *J Appl Physiol* 1989; **67:** 2006–2013.
36 Green JH. *The Autonomic Nervous System and Exercise.* Chapman & Hall: London 1990, pp 126–128.
37 Van Loan MD, McCluer S, Loftin JM, Boileau RA. Comparison of physiological responses to maximal arm exercise among able-bodied, paraplegics and quadriplegics. *Paraplegia* 1987; **25:** 397–405.

Development/Plasticity/Repair

Growth Factor Treatment and Genetic Manipulation Stimulate Neurogenesis and Oligodendrogenesis by Endogenous Neural Progenitors in the Injured Adult Spinal Cord

Yasuo Ohori,[1,3,4] Shin-ichi Yamamoto,[3,4] Motoshi Nagao,[1] Michiya Sugimori,[1] Naoya Yamamoto,[4] Kozo Nakamura,[3] and Masato Nakafuku[1,2,5]

[1]Division of Developmental Biology, Cincinnati Children's Hospital Research Foundation, Cincinnati, Ohio 45229-3039, [2]Departments of Pediatrics and Neurosurgery, University of Cincinnati College of Medicine, Cincinnati, Ohio 45267-0521, [3]Department of Orthopaedic Surgery, The University of Tokyo Graduate School of Medicine, Bunkyo-ku, Tokyo 113-0033, Japan, [4]Division of Motor Dysfunction, Research Institute, National Rehabilitation Center, Tokorozawa, Saitama 359-8555, Japan, and [5]Solution Oriented Research for Science and Technology, Japan Science and Technology Agency, Chuo-ku, Tokyo 103-0027, Japan

Neurons and oligodendrocytes are highly vulnerable to various insults, and their spontaneous replacement occurs to only a limited extent after damage in the adult spinal cord. The environment of injured tissue is thus thought to restrict the regenerative capacity of endogenous neural stem/progenitor cells; strategies for overcoming such restrictions remain to be developed. Here, we combined growth factor treatment and genetic manipulation to stimulate neurogenesis and oligodendrogenesis by endogenous progenitors *in vivo*. The recombinant retrovirus pMXIG, which was designed to coexpress green fluorescent proteins (GFPs) and a neurogenic/gliogenic transcription factor, was directly injected into the injured spinal cord parenchyma to manipulate proliferative cells *in situ*. We found that cells expressing Olig2, Nkx2.2, and NG2 were enriched among virus-infected, GFP-positive (GFP$^+$) cells. Moreover, a fraction of GFP$^+$ cells formed neurospheres and differentiated into neurons, astrocytes, and oligodendrocytes *in vitro*, demonstrating that GFP retroviruses indeed infected endogenous neural progenitors *in vivo*. Neuronal differentiation of control virus-infected cells did not occur at a detectable level in the injured spinal cord. We found, however, that direct administration of fibroblast growth factor 2 and epidermal growth factor into lesioned tissue could induce a significant fraction of GFP-labeled cells to express immature neuronal markers. Moreover, retrovirus-mediated overexpression of the basic helix-loop-helix transcription factors Neurogenin2 and Mash1, together with growth factor treatment, enhanced the production and maturation of new neurons and oligodendrocytes, respectively. These results demonstrate that endogenous neural progenitors can be manipulated to replace neurons and oligodendrocytes lost to insults in the injured spinal cord.

Key words: stem cell; regeneration; repair; spinal cord injury; neurogenesis; oligodendrocyte; bHLH factor; growth factor

Introduction

The adult mammalian CNS is highly vulnerable to various insults. It has long been thought that such vulnerability is attributable to the lack of cell sources for replacing dead and/or damaged cells (Horner and Gage, 2000). Many lines of previous studies, however, have revealed that neural stem and other progenitor cells [herein collectively called neural progenitor cells (NPCs)] persist in the adult CNS (Q. Cao et al., 2002). In fact, neurogenesis and gliogenesis continue in some regions of the adult brain in various species, including humans (Goldman, 2004).

Such continuous cell genesis, however, is confined to only a few areas under physiological conditions, and moreover, regeneration of new cells appears to be very limited even after damage in most regions of the CNS (Goldman, 2004). In particular, the adult spinal cord has been considered to be one of the most restrictive regions in which NPCs can contribute to cell replacement after injury (Q. Cao et al., 2002; Dobkin and Havton, 2004). Previous cell culture studies have demonstrated that the adult spinal cord contains an abundant source of endogenous NPCs (Weiss et al., 1996; Johansson et al., 1999; Shihabuddin et al.,

Received Jan. 11, 2006; revised Sept. 5, 2006; accepted Oct. 10, 2006.

This work was supported in part by the Ohio Eminent Scholar Award of the Sate of Ohio, the Solution Oriented Research for Science and Technology Program, Japan Science and Technology Agency, and grants-in-aids from The Ministry of Education, Culture, Sports, Science and Technology, Japan. We thank Drs. T. Kitamura, K. Miyazono, Y. Gotoh, Y. Ihara, and I. Dobashi for reagents and technical assistance. We also thank Drs. C. Wylie, T. Boat, A. Seichi, S. Tanaka, Y. Tajiri, T. Miura, and T. Ogata, and the members of our laboratories for encouragement and support. We declare that the authors of this study have no financial conflicts of interest that might be construed to influence the results or interpretation of this study.

Correspondence should be addressed to Dr. Masato Nakafuku, Division of Developmental Biology, Cincinnati Children's Hospital Research Foundation, 3333 Burnet Avenue, Cincinnati, OH 45229-3039. E-mail: masato.nakafuku@cchmc.org.

DOI:10.1523/JNEUROSCI.3127-06.2006

 0270-6474/06/2611948-13$15.00/0

2000; Yamamoto et al., 2001a; Martens et al., 2002). Nevertheless, production of new neurons and oligodendrocytes by such endogenous cells occurs to only a very limited extent after injury *in vivo* (McTigue et al., 1998, 2001; Johansson et al., 1999; Yamamoto et al., 2001a,b; Kojima and Tator, 2002; Zai and Wrathall, 2005; Horky et al., 2006; Yang et al., 2006). Furthermore, cell transplantation studies have demonstrated that exogenous NPCs, which retain strong neurogenic and/or oligodendrogenic activities *in vitro*, differentiate only very poorly when grafted into the spinal cord (Chow et al., 2000; Shihabuddin et al., 2000; Q. L. Cao et al., 2001, 2002; Han et al., 2002, 2004; Hill et al., 2004; Enzmann et al., 2005). Thus, the environment of the spinal cord appears to be highly restrictive for differentiation of NPCs. If this environmental restriction can be relieved by certain manipulations, endogenous NPCs may be able to supply new neurons and oligodendrocytes, which in turn may contribute to the reconstruction of local circuitry and facilitate regeneration of long-distance axonal tracts (Schwab, 2002; Dobkin and Havton, 2004). However, such strategies to manipulate endogenous NPCs remain unexplored to date.

In this study, we tested two strategies to manipulate neuronal and glial differentiation of endogenous NPCs *in vivo*. The first was direct administration of a mixture of growth factors (GFs), fibroblast growth factor 2 (FGF2) and epidermal growth factor (EGF), into injured tissue and the second was virus-mediated overexpression of the transcription factors Neurogenin2 (Ngn2) and Mash1. We show that the combination of these manipulations can stimulate the production of new neurons and oligodendrocytes by endogenous NPCs in the injured spinal cord.

Materials and Methods

Spinal cord injury. Young adult Sprague Dawley rats (7–9 weeks of age and weighing 250–330 g) were used in all experiments. All experimental procedures were performed according to the guidelines of the Institutional Animal Care and Use Committee and National Institutes of Health. Rats were anesthetized with 50 mg of ketamine HCl and 5 mg of xylazine (100 and 20 mg/ml, respectively; Phoenix Pharmaceuticals, St. Joseph, MO) per kilogram of body weight. Laminectomy and complete transection of the spinal cord at the tenth thoracic (T10) level were performed as described previously (Yamamoto et al., 2001a,b).

Growth factor treatment and retrovirus infection in vivo. Recombinant retroviruses pMXIG and pMXIG-Ngn2, which are designed to express green fluorescent protein (GFP) as a marker for infected cells, were described previously (Morita et al., 2000; Yamamoto et al., 2001b). pMXIG-Mash1 was constructed by inserting the full-length cDNA for rat Mash1 (Torii et al., 1999) into the pMXIG vector. For virus infection *in vivo*, a 30 μl solution of artificial CSF (aCSF) containing high-titer retroviruses (2×10^8 colony-forming unit/ml), 0.1 mg/ml rat serum albumin (Sigma, St. Louis, MO), and 4 μg/ml polybrene (Sigma) was injected manually into three different locations (10 μl each) of the transected spinal cord parenchyma using Hamilton syringes (Hamilton, Reno, NV). In some experiments, recombinant human FGF2 (1 μg; Peprotech, Rocky Hill, NJ), mouse EGF (1 μg; Roche, Indianapolis, IN), and human brain-derived neurotrophic factor (BDNF) (2 μg; Sigma) were premixed and coinjected with retroviruses. An equivalent amount of rat serum albumin was used as control. To label proliferating cells, 5-bromo-2′deoxyuridine (BrdU) (150 mg/kg of body weight; Sigma) dissolved in 0.9% sterile saline was injected intraperitoneally twice a day for 3 d between day after injury 0 (DAI0) and DAI2. The first administration of BrdU was performed immediately after virus injection, and subsequently repeated every 12 h.

In vitro *culture.* Spinal cord stumps ~4 mm-long both rostral and caudal from the lesion epicenter were subjected to *in vitro* culture as described previously (Yamamoto et al., 2001a,b) with some modifications. In brief, the harvested tissue was cut into small pieces in ice-cold aCSF containing the following (in mM): 124 NaCl, 5 KCl, 1.3 $MgCl_2$, 2 $CaCl_2$, 26 $NaHCO_3$, and 10 D-glucose. Subsequently, the tissue was dissociated by incubation with 0.1% (w/v) trypsin (Sigma), 0.67 mg/ml hyaluronidase (Sigma), and 0.1 mg/ml deoxyribonuclease I (Roche) in aCSF at 37°C for 30 min, with aeration with 95% O_2/5% CO_2. Trypsin was neutralized with 0.7 mg/ml ovamucoid (Sigma) and the resultant tissue suspension was triturated mechanically to yield a single cell suspension. In some experiments, the resultant cells were immediately seeded onto poly-D-lysine (PDL; 100 μg/ml; Sigma)-coated eight-well chambers (Nalge Nunc International, Rochester, NY) and subjected to immunostaining 2 h after plating.

To initiate neurosphere culture, fragmented neuropiles and other debris were removed from the above-described dissociated single cell suspension by filtration through serum cushion and a sterile nylon mesh (40 μm pore diameter; Becton, Dickinson and Company, Franklin Lakes, NJ) (Yamamoto et al., 2001b). The resultant single cells were seeded at the density of 2×10^4 cells/ml in a growth medium [1:1 mixture of DMEM and F-12 medium supplemented with B-27 and N2 culture supplements (Invitrogen, Carlsbad, CA), 20 ng/ml bovine FGF2, 20 ng/ml mouse EGF, 20 ng/ml human platelet-derived growth factor (R & D Systems, Minneapolis, MN), 2 μg/ml heparin (molecular mass 3000; Sigma), 1 mg/ml bovine serum albumin (Sigma), and 100 μM 2-mercaptoethanol (Sigma)]. Culture dishes were coated with poly [2-hydroxyethyl methacrylate] (Sigma) to prevent cell attachment (Yamamoto et al., 2001b). At day 14 *in vitro* (DIV14), forming floating neurospheres were collected and subjected to either serial passages under the same condition or differentiation culture. Under these conditions, 0.9 ± 0.1% ($n = 6$ independent experiments) of initially seeded viable cells formed neurospheres, and this frequency was maintained in subsequent four passages.

To induce differentiation into neurons and glia, neurospheres grown in the presence of GFs were seeded onto PDL-coated eight-well chambers, either as cell aggregates or dissociated single cells, at a density of 2×10^4 cells per well, and subsequently cultured in the above medium without GFs or heparin for 6 d. In some experiments, the following peptide factors were added to the culture medium: human bone morphogenetic protein 4 (BMP4; 10 ng/ml; R & D systems), mouse noggin (100 ng/ml; R & D Systems), human ciliary neurotrophic factor (CNTF; 50 ng/ml; Sigma), and human BDNF (50 ng/ml; Sigma). To count cell numbers, cell nuclei were stained with 1 μg/ml 4′,6-diamidino-2-phenylindole (DAPI; Invitrogen).

Retrovirus infection in vitro. The full-length cDNAs for mouse Smad6 and Samd7, and a dominant-negative form of mouse STAT3 (Kamakura et al., 2004) were kind gift from Drs. K Miyazono and Y. Gotoh (The University of Tokyo, Tokyo, Japan), respectively, and cloned into pMXIG vector. Primary neurospheres collected at DIV14 were subjected to virus infection as described previously (Yamamoto et al., 2001b). Infected cells were maintained in floating culture for a week, during which ~10% of the cells expressed GFP. The resultant secondary neurospheres were dissociated, seeded onto PDL-coated chambers, and incubated for additional 2 d without GFs to induce differentiation.

Immunostaining. Affinity-purified rabbit polyclonal antibodies (pAbs) against nestin (diluted 1:1000), Olig2 (1:2000), Ngn2 (1:5000), and Sox2 (1:1000) were described previously (Yamamoto et al., 2001a,b). Rabbit antibody for microtubule-associated protein 2 (MAP2) (react with c subunit, 1:4000) was generous gift from Dr. Y. Ihara (The University of Tokyo) (Yamamoto et al., 2001b). Mouse monoclonal antibodies (mAbs) against nestin (Rat401, 1:500), Nkx2.2 (74.5A5, 1:1000), HB9 (81.5C10, 1:50), Islet1 (39.4D5, 1:50), Lim1 (4F2, 1:50), Lim3 (67.4E12, 1:50), and RIP (Rip, 1:100) were obtained from the Developmental Studies Hybridoma Bank of the University of Iowa. Other antibodies were purchased from commercial sources: GFP [mouse mAb, 1:500; rabbit pAb, 1:5000 (Invitrogen); and rat mAb, 1:5000 (Nacalai Tesque, Kyoto, Japan)], BrdU [mouse mAb, 1:200 (BD Biosciences, Franklin Lakes, NJ), and rat mAb (Oxford Biotechnology, Oxford, UK)], HuC/D (mouse mAb, 1:1000; Invitrogen), MAP2 (mouse mAb clone AP20 detecting a and b subunits, 1:100; Roche), β-tubulin type III (TuJ1) (mouse mAb, 1:5000; Babco, Richmond, CA), NeuN (mouse mAb, 1:200; Millipore, Temecula, CA), glial fibrillary acidic protein (GFAP) [mouse mAb, 1:1000 (Millipore) and rabbit pAb, 1:1000 (Sigma)], NG2 (mouse mAb,

1:1000, and rabbit pAb, 1:1000; Millipore), myelin basic protein (MBP) (mouse mAb, 1:1000; Millipore), proteolipid protein (PLP) (mouse mAb, 1:100; Millipore), O4 (mouse IgM mAb, 1:400; Millipore), galactocerebroside (GalC) (mouse mAb, 1:200; Millipore), glutathione-S-transferase π (GST-π) (mouse mAb, 1:50; Becton Dickinson), OX42 (mouse mAb clone CD11b, 1:50; Serotec, Raleigh, NC), RECA-1 (mouse mAb, 1:5; Serotec), choline acetyltransferase (ChAT) (rabbit pAb, 1:500; Millipore), γ-aminobutyric acid (GABA) (rabbit pAb, 1:500; Sigma), synaptophysin (mouse mAb, 1:100; Roche), and Mash1 (mouse mAb, 1:200; BD Biosciences).

For immunohistochemistry of tissue sections, rats were killed and fixed by intracardial perfusion of 4% (w/v) paraformaldehyde (Acros, Geel, Belgium) in phosphate-buffered saline. Isolated spinal cord tissues were cryoprotected with 10–30% (w/v) sucrose (Fisher Scientific, Pittsburgh, PA), and embedded into OCT compound (Sakura Finetek USA, Torrance, CA). Staining was visualized with appropriate sets of secondary antibodies conjugated with Alexa Fluor 350, 488, 568, 594, and 633 (1:200; Invitrogen) as described previously (Yamamoto et al., 2001b; Nakatomi et al., 2002).

To examine the total number of virus-infected cells in injured spinal cords, 14-μm-thick serial transverse sections were prepared from 5-mm-long spinal cord stumps (2.5 mm each for rostral and caudal to the lesion epicenter). Among these serial sections, representative 12 sections, at least 280 μm apart from each other, were subjected to immunostaining with GFP antibody. The number of GFP$^+$ cells in the entire area of each section was counted manually under Zeiss (Oberkochen, Germany) fluorescence microscope AxiophotoII. The sum of these numbers was multiplied with the number of total sections obtained from each samples (~360 sections), and then divided by 12 to yield the total number of GFP$^+$ cells per spinal cord.

To examine the coexpression of various cell type-specific markers in GFP$^+$ cells, six representative sections from the above serial transverse sections were double or triple stained for GFP and relevant markers. The entire area of the all sections was examined manually under fluorescence microscope. To further validate the costaining of multiple makers in single cells, 1–2 representative sections from each animal was further examined by confocal Z-sectioning at an interval of 1.0 μm under Zeiss microscope LSM-501 as described previously (Nakatomi et al., 2002). Only cells that appeared to retain the intact soma and nuclei within a given section, which was judged according to the staining pattern of GFP, were counted.

To compare the coexpression of various markers in GFP$^+$ and BrdU$^+$ cells, 14-μm-thick serial parasagittal sections were prepared from 8-mm-long spinal cord stumps (4 mm each for rostral and caudal to the lesion epicenter). Among these sections, six representative sections, which were at least 280 μm apart from each other, were subjected to immunostaining. Costaining of individual GFP$^+$ and BrdU$^+$ cells with other markers was examined as described above by scanning the entire area of individual sections. As for BrdU$^+$ cells, cells that retained oval or round nuclear staining for BrdU were included for counting.

Statistical analysis. The quantitative results were expressed as mean ± SD, and the numbers of replicated experiments are shown in text or figure legends. Statistical analyses were performed with two-tailed unpaired *t* test or one-way ANOVA.

Results

Retrovirus-mediated genetic labeling of proliferative cells in the injured spinal cord

Previous studies have demonstrated that endogenous NPCs proliferate in response to spinal cord injury (Johansson et al., 1999; Yamamoto et al., 2001a,b; Kojima and Tator, 2002; Horky et al., 2006). As a tool to genetically manipulate these proliferating progenitors *in situ*, we used replication-incompetent, recombinant retroviruses. Retroviruses almost exclusively infect dividing cells (Leber and Sanes, 1991; Horky et al., 2006). Thus, when directly administered to injured spinal cords, they are expected to infect proliferating NPCs together with other cell types. The retrovirus vector pMXIG used in this study was designed to express GFP so that virus-infected cells were detected as GFP-positive (GFP$^+$) cells (Morita et al., 2000; Yamamoto et al., 2001a,b).

Immediately after transection at the thoracic level, a small volume of high-titer pMXIG viruses was directly injected into the damaged parenchyma. At DAI3, virus-infected, GFP$^+$ cells were detected locally around the injected site. By DAI7, however, many GFP$^+$ cells spread out to broader areas, reaching at a distance of ~2.5 mm from the lesion epicenter both rostrally and caudally (Fig. 1*A*). Some GFP-labeled cells were detected up to 4 mm away from the lesion. In the areas proximal (<1 mm) to the lesion, GFP$^+$ cells distributed in both the gray and white matters, which were revealed by costaining of GFP with the myelin protein MBP (Fig. 1*B*). At locations distal (>2 mm) to the lesion, however, more GFP$^+$ cells were detected in the MBP$^+$ white matter than in the gray matter where NeuN$^+$ neurons were densely populated (Fig. 1*C*). Given such widespread distribution of virus-infected cells, we included 8-mm-long spinal cord stumps encompassing the T8 to T12 columns for quantitative analyses. As a whole, $2.87 \pm 1.28 \times 10^4$ and $1.50 \pm 0.67 \times 10^4$ GFP$^+$ cells were detected at DAI3 and DAI7, respectively, per spinal cord ($n = 3$) after infection with control viruses.

Both FGF2 and EGF are required for proliferation of adult spinal cord NPCs *in vitro* and *in vivo* (Weiss et al., 1996; Johansson et al., 1999; Yamamoto et al., 2001a,b; Kojima and Tator, 2002; Martens et al., 2002). Thus, to stimulate their proliferation *in situ*, we administered a mixture of FGF2 and EGF together with retroviruses (1 μg each per animal). This GF treatment resulted in 1.6- and 2.7-fold increases in the number of GFP$^+$ cells at DAI3 and DAI7, respectively ($4.67 \pm 2.10 \times 10^4$ cells at DAI3 and $4.00 \pm 1.80 \times 10^4$ cells at DAI7 per spinal cord, $n = 3$). Moreover, the survival rate of GFP$^+$ cells between DAI3 and DAI7 was significantly higher in GF-treated animals (85.6%) than that in untreated animals (52.3%) ($p < 0.01$ in two-tailed unpaired *t* test). These results suggest that GFs stimulated both proliferation and survival of virus-infected cells *in vivo*. Treatment with either FGF2 or EGF alone, or their combination at a lower dose (0.1 μg each) resulted in a much smaller increase (<1.2-fold) in the number of GFP$^+$ cells at DAI7 (data not shown), suggesting a dose-dependent, combinatorial effect of FGF2 and EGF. We did not observe, however, any significant difference in the overall distribution pattern of GFP$^+$ cells within injured tissue between GF-treated and untreated animals. The extent of tissue damage and overall staining patterns of NeuN, MBP, GFAP, and OX42 also appeared to be similar between the two groups (data not shown). Thus, although GFs have been shown to exert pleiotropic effects in the injured spinal cord, including modulation of inflammatory responses, glial scar formation, and survival of neurons and glia (Cheng et al., 1996; Lee et al., 1999; Teng et al., 1999; Rabchevsky et al., 2000; Kojima and Tator, 2002; Meijs et al., 2004), we focused our analyses on their effects on the differentiation of GFP-labeled cells in this study.

Properties of GFP virus-labeled cells *in vivo*

We next examined the early phenotypes of GFP$^+$ cells in injured tissue. The infectability of retroviruses *in vivo* is lost in a relatively short period of time (Leber and Sanes, 1991; Horky et al., 2006). Therefore, when pMXIG viruses were administered immediately after transection, they are thought to preferentially label cells that proliferated early after injury. We compared such cells with those marked by the BrdU labeling method. Intraperitoneal administration of BrdU was initiated right after virus injection and subsequently repeated twice a day for 3 d. In these animals, 28 ± 6.2% of GFP$^+$ cells were colabeled with BrdU at DAI3, indicating

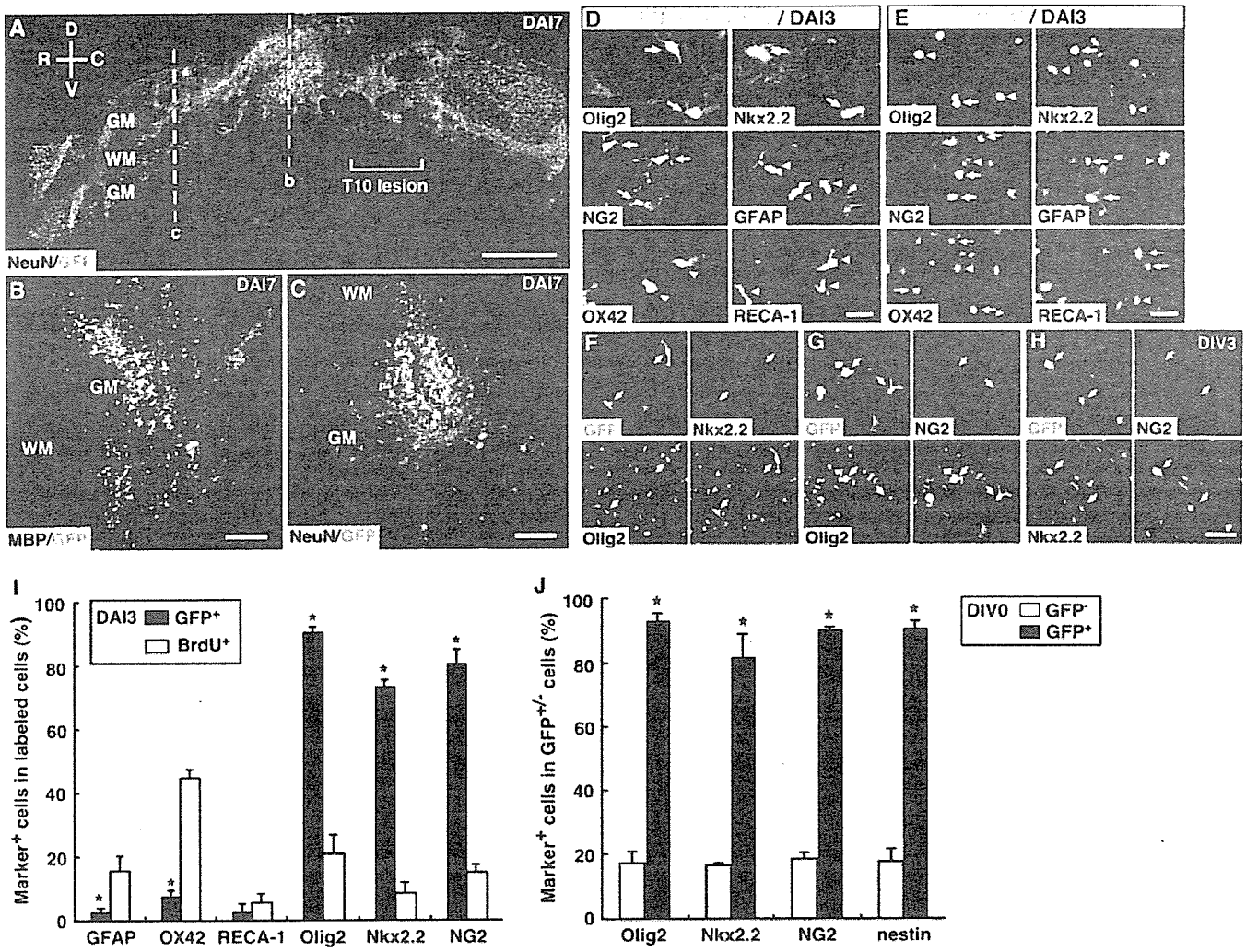

Figure 1. Distribution patterns and phenotypes of GFP virus-infected cells in the injured spinal cord. ***A–C***, Micrographs of parasagittal (***A***) and transverse (***B***, ***C***) sections of spinal cords infected with GFP-expressing pMXIG recombinant retrovirus at DAI7. Distribution of virus-infected GFP cells (green) in the gray matter (GM) and white matter (WM) (red) was revealed by coimmunostaining of GFP with NeuN (***A***, ***C***) and MBP (***B***), respectively. Dorsal (D) is up, ventral (V) is down, rostral (*R*) is left, and caudal (*C*) is right. Bracket in ***A*** shows the location of the lesion epicenter at the T10 level. Right and left dashed lines in ***A*** indicate the approximate locations of the transverse sections shown in ***B*** and ***C***, respectively. ***D***, ***E***, Micrographs of double immunostaining of GFP$^+$ (***D***) and BrdU$^+$ (***E***) cells (green) with various cell type-specific markers (red) at DAI3. Arrows and arrowheads indicate GFP$^+$ cells positive and negative, respectively, for markers shown in each panel. ***F–H***, Coexpression of Olig2, Nkx2.2, and NG2, and in GFP$^+$ cells. Dissociated single cells isolated from spinal cords treated with GFs and GFP viruses were subjected to triple immunostaining at DAI3. Arrows indicate cells positive for respective markers (shown in green, red, and blue in each panel), and the bottom-right panels are merged images. ***I***, Histograms comparing the percentages of marker-positive cells in total GFP-labeled (filled bars) and BrdU-labeled (open bars) cells at DAI3. Data are mean ± SD based on three independent experiments shown in ***D*** and ***E*** (*$p < 0.001$ compared with BrdU-labeled cells). ***J***, Histograms comparing the expression of Olig2, Nkx2.2, NG2, and nestin between GFP$^+$ (filled bars) and GFP$^-$ (open bars) cell populations at DIV0. The percentages of GFP$^+$ and GFP$^-$ cells expressing respective markers were quantified (mean ± SD; $n = 3$–5 animals; *$p < 0.01$ compared with GFP$^-$ cells). Scale bars: ***A***, 1.0 mm; ***B***, ***C***, 200 μm; ***D***, ***E***, 50 μm; (in ***H***) ***F–H***, 20 μm.

that GFP viruses indeed infected a population of proliferative cells *in vivo*. However, GFP$^+$/BrdU$^+$ cells comprised only 6% of total BrdU$^+$ cells, suggesting that the majority of BrdU-labeled cells proliferated after the period of virus infection. Consistent with our previous study (Yamamoto et al., 2001a), the major fractions of these BrdU$^+$ cells were OX42$^+$ microglia and other inflammatory cells (44.7%), RECA-1$^+$ vascular endothelial cells (5.6%), and GFAP$^+$ astrocytes (15.7%) (Fig. 1*E*, arrows, *I*); these cells, as a whole, comprised 66.0% of total BrdU$^+$ cells. In contrast, these cell types were rather minor among GFP$^+$ cells (14.2% in total) (Fig. 1*D*,*I*), suggesting that cells other than these cell types were preferentially infected with viruses.

It has been shown that cells expressing the proteoglycan NG2 are one of the predominant proliferative cell types in both the intact and injured spinal cord (Horner et al., 2000; Ishii et al., 2001; McTigue et al., 2001; Dawson et al., 2003; Horky et al., 2006). Previous studies have also demonstrated that cells expressing the transcription factors Olig2 and Nkx2.2 comprise subpopulations of proliferative cells in injured tissue (Yamamoto et al., 2001b; Han et al., 2004; Watanabe et al., 2004; Talbott et al., 2005). We found that the vast majority of GFP$^+$ cells detected at DAI3 expressed Olig2 (90.7 ± 1.5%), Nkx2.2 (73.7 ± 2.1%), and NG2 (80.7 ± 4.2%; $n = 3$ animals) (Fig. 1*D*,*I*). These cells did not overlap with OX42$^+$, RECA-1$^+$, or GFAP$^+$ cells (data not shown) (Yamamoto et al., 2001b; Watanabe et al., 2002, 2004; Talbott et al., 2005). However, the percentages of cells positive for these three markers among BrdU$^+$ cells were significantly lower than those among GFP$^+$ cells. Given the difference in the period of cell labeling, these suggest that cells expressing NG2, Olig2, and Nkx2.2 are predominant proliferative cell types early after injury. In line with this idea, when BrdU was administered only once at DAI0, the fractions of Olig2$^+$ and NG2$^+$ cells among total

BrdU$^+$ cells significantly increased (59.6 ± 3.2 and 53.3 ± 4.7%, respectively; $n = 3$ animals), whereas the percentage of OX42$^+$/BrdU$^+$ cells became much lower (23.4 ± 1.1%) compared with those after repetitive injections for 3 d. Conversely, when GFP viruses were administered at both DAI0 and DAI2, the percentage of Olig2$^+$/GFP$^+$ cells was significantly lower than that detected after single administration (37.1 vs 90.7%; $n = 2$ animals). These results are in agreement with the recent report by Horky et al. (2006) in that NG2$^+$ cells proliferate early after injury, which is followed by expansion of OX42$^+$ and GFAP$^+$ cells at later stages. Given these results, we chose the condition of single virus injection in subsequent studies.

The above results suggested that the majority of GFP$^+$ cells coexpressed all three markers. We further addressed this issue using dissociated single cell preparations (Fig. 1*F-H,J*). To avoid possible regional variability, cells were recovered from 8 mm spinal cord stumps where the entire population of GFP$^+$ cells distributed. In such preparations, GFP$^+$ cells comprised only 1.3 ± 0.6% ($n = 6$ animals) of total cells at DAI3. Among these GFP$^+$ cells, 93.3 ± 2.1 and 82.0 ± 7.0% were Olig2$^+$ and Nkx2.2$^+$, respectively (Fig. 1*F–H,J*). Likewise, NG2$^+$ cells were highly enriched in the GFP$^+$ population (90.7 ± 0.6%). Furthermore, a series of triple staining demonstrated that the majority (>80%) of GFP$^+$ cells were positive for all three markers (Fig. 1*F–H*). Most of these cells also expressed nestin and Sox2, commonly used markers for undifferentiated NPCs (Fig. 1*J*) (data not shown). These properties of GFP$^+$ cells were essentially identical between GF-treated and untreated animals at DAI3. Such cells, however, were <20% among GFP$^-$ cells that represented the total cell population in injured tissue (Fig. 1*J*).

We next sought to examine the frequency of NG2$^+$/Olig2$^+$/Nkx2.2$^+$ cells, which comprised the major fraction of virus-infected cells (Fig. 2). Because triple staining of these three markers could not be performed because of technical reasons, we conducted a series of double staining. NG2$^+$ cells comprised 6.5 ± 1.1% of total cells in the intact spinal cord, and among these NG2$^+$ cells, NG2$^+$/Olig2$^+$ and NG2$^+$/Nkx2.2$^+$ cells were 43 and 60%, respectively (Fig. 2*A*). Likewise, only a fraction of Olig2$^+$ cells expressed NG2 and Nkx2.2 [20% (2.8 ÷ 14.2) and 35% (5.0 ÷ 14.2), respectively], and only 74% (5.0 ÷ 6.8) and 57% (3.9 ÷ 6.8) of Nkx2.2$^+$ cells coexpressed Olig2 and NG2, respectively. Thus, in terms of the coexpression of these markers, heterogeneous cell types coexisted in the spinal cord, consistent with the results of previous studies (Yamamoto et al., 2001b; Watanabe et al., 2004; Talbott et al., 2005; Kitada and Rowitch, 2006). Using the Venn diagram based on these results, we estimated that NG2$^+$/Olig2$^+$/Nkx2.2$^+$ cells comprised 2.1–2.8% of the total cells in the intact spinal cord (Fig. 2*B*), which corresponded to 30–40% of total NG2$^+$ cells. The fact that the vast majority of GFP$^+$ virus-labeled cells coexpressed three markers indicates that such triple positive cells indeed exist *in vivo*. After transection injury, this cell population increased to 3.9–6.0% mainly because of a net increase (2.3-fold) in the number of NG2$^+$ cells as observed under other injury conditions such as contusion and demyelination (Watanabe et al., 2004; Talbott et al., 2005; Horky et al., 2006; Kitada and Rowitch, 2006).

A

tissue	NG2$^+$	Olig2$^+$	Nkx2.2$^+$	NG2$^+$/Olig2$^+$	NG2$^+$/Nkx2.2$^+$	Olig2$^+$/Nkx2.2$^+$	NG2$^+$/ Olig2$^+$/Nkx2.2$^+$
intact	6.5±1.1	14.2±0.6	6.8±1.0	2.8±0.4 (43.1)	3.9±0.8 (60.0)	5.0±0.6	2.1-2.8
DAI3	14.9±1.5	14.6±1.4	9.1±0.1	6.0±1.6 (40.3)	6.4±0.1 (43.0)	6.6±2.1	3.9-6.0

B

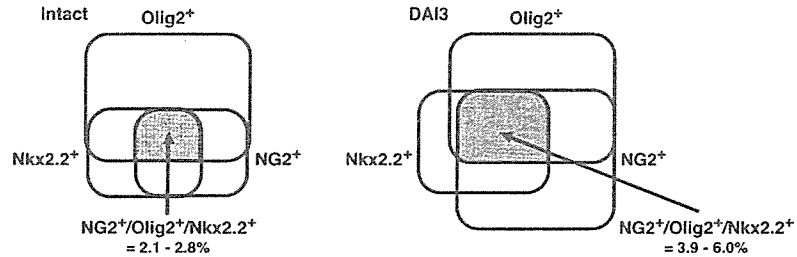

Figure 2. Occurrence of cells expressing NG2, Olig2, and Nkx2.2 in the spinal cord. ***A***, Percentages of NG2$^+$, Olig2$^+$, and Nkx2.2$^+$ cells in total cells, and also cells double positive for respective markers are shown. Single and double positive cells were quantified by a series of double staining of dissociated cells obtained from the intact and injured (DAI3) spinal cords (mean ± SD; $n = 2$–3 animals). Data in parenthesis show the percentages of Olig2$^+$ and Nkx2.2$^+$ cells among total NG2$^+$ cells. ***B***, Venn diagram showing the relationships among NG2$^+$, Olig2$^+$, and Nkx2.2$^+$ cells in the intact and injured spinal cord. Based on the data in ***A***, the frequency of cells coexpressing all three markers among total spinal cord cells is estimated.

Neurosphere formation by GFP virus-labeled cells

We next asked whether cells infected with GFP viruses *in vivo* contained NPCs. Here, we operationally define NPCs as the cells that can grow as neurospheres in the presence of GFs and differentiate into neurons and glia after removal of GFs *in vitro* (Weiss et al., 1996; Johansson et al., 1999; Yamamoto et al., 2001b; Martens et al., 2002). Injured spinal cords treated with GFP viruses and GFs were dissociated into single cells at DAI3, and NPCs were subsequently expanded as floating neurospheres. Although the frequency of GFP$^+$ cells among initial viable cells was very low (1.3 ± 0.6% at DIV0; $n = 6$), they were significantly enriched (6.3-fold) in neurosphere culture; 8.2 ± 1.2% of total cells recovered as neurospheres were GFP$^+$ at DAI14 ($n = 4$; $p < 0.01$ compared with DAI0 in two-tailed unpaired t test) (Fig. 3*A–C*). About one-third of GFP$^+$ neurospheres were entirely composed of GFP$^+$ cells (Fig. 3*B,B'*), and they repeatedly formed GFP$^+$ spheres after passages (data not shown). Given the low frequency of GFP$^+$ cells in the original samples subjected to culture, such purely GFP$^+$ neurospheres were likely to have derived from single GFP$^+$ cells. The majority of these GFP$^+$ cells in primary neurospheres expressed Olig2 and Nkx2.2 (90.5 ± 6.4% for Olig2 and 81.7 ± 4.2% for Nkx2.2; $n = 3$) (Fig. 3*D,E,H*). About one-third of GFP$^+$ cells were also NG2$^+$ (32.0 ± 6.6%; $n = 3$) (Fig. 3*F,H*) and nestin$^+$ (Fig. 3*G*). Importantly, cells positive for these markers were also the predominant cell type in virus uninfected, GFP$^-$ neurospheres (Fig. 3*H*), despite that such cells were rather minor among GFP$^-$ cells before neurosphere formation (Fig. 1*J*).

After removal of GFs, both GFP$^+$ and GFP$^-$ neurospheres gave rise to TuJ1$^+$ neurons, GFAP$^+$ astrocytes, and O4$^+$ oligodendrocytes (Fig. 3*I,I'*). By a series of triple staining, we confirmed that most (>95%) of the GFP$^+$ spheres composed entirely of GFP$^+$ cells contained all three neural lineages (data not shown). Because the ratio of neurons and glia was variable among individual neurospheres, the percentages of cells expressing neuronal and glial markers were quantified using preparations of

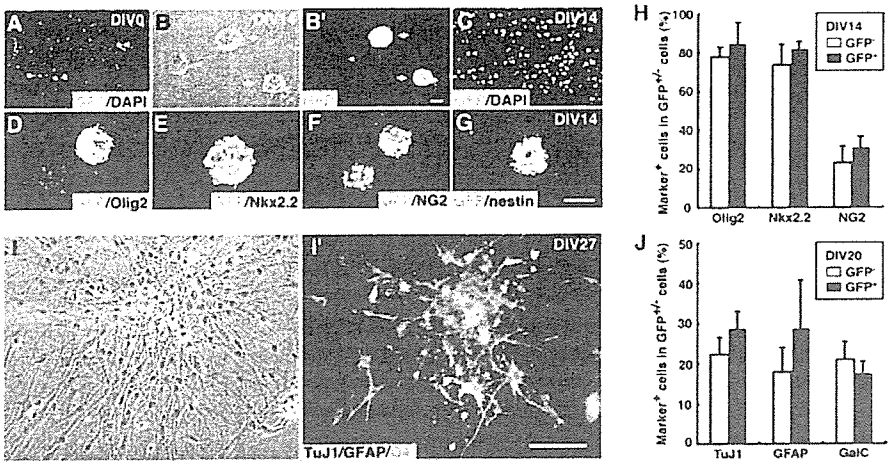

Figure 3. Neurosphere formation by GFP virus-labeled cells *in vitro*. ***A–C***, *In vitro* expansion of GFP $^+$ cells as neurospheres. ***A*** and ***C*** show immunostaining of GFP (green) and nuclear staining with DAPI (blue) in dissociated single cells at DIV0 and DIV14, respectively, in neurosphere culture. The frequency of GFP $^+$ cells in the initial cell population at DIV0 was very low (***A***, arrowheads), but they were highly enriched in neurospheres at DIV14 (***C***, arrowheads). ***B*** and ***B′*** are bright-field and fluorescence images of GFP $^+$ (arrows) and GFP $^-$ (arrowhead) neurospheres, respectively, at DIV14. ***D–G***, The expression of Olig2, Nkx2.2, NG2, and nestin (red) in GFP $^+$ neurospheres (green) at DIV14. ***H***, Histograms comparing the percentages of Olig2 $^+$, Nkx2.2 $^+$, and NG2 $^+$ cells in total GFP $^+$ (filled bars) and GFP $^-$ (open bars) neurosphere cells at DIV14 (mean ± SD; $n = 3–5$ independent cultures). ***I***, ***I′***, Differentiation of neurosphere cells. Bright-field (***I***) and fluorescence (***I′***) images of a secondary neurosphere stained for TuJ1 (red), GFAP (blue), and O4 (green). Cells were induced to differentiate for 6 d between DIV21 and DIV26 on a PDL-coated glass chamber. ***J***, Differentiation of GFP $^+$ and GFP $^-$ neurosphere cells into neurons and glia. Primary neurospheres at DIV14 were dissociated into single cells and induced to differentiate in monolayer for 6 d. The percentages of GFP $^+$ and GFP $^-$ cells expressing respective neuronal and glial cell markers were quantified (mean ± SD; $n = 3–6$ independent cultures). Scale bars: (in ***G***) ***A***, ***C***, ***D–G***, 100 μm; (in ***B′***) ***B***, ***B′***, 50 μm; (in ***I′***) ***I***, ***I′***, 20 μm.

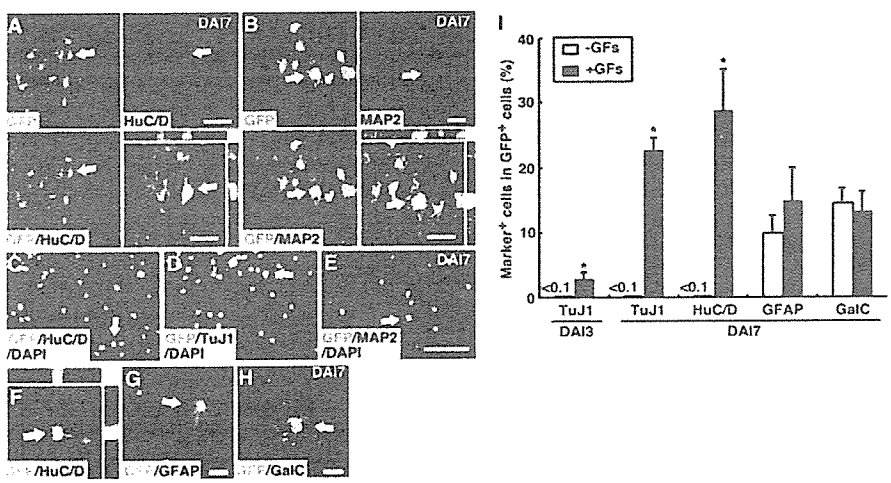

Figure 4. Induction of new neurons by GFs in injured spinal cords. ***A***, ***B***, Micrographs showing the expression of the neuronal markers HuC/D (***A***) and MAP2 (***B***) (red) in GFP $^+$ cells (arrows) at DAI7. The bottom-right panel in each set shows a three-dimensional digital image of the cell indicated by arrows in the other panels. ***C–H***, Expression of various neuronal and glial cell markers in GFP $^+$ cells at DAI7. Dissociated single cells prepared from GF-treated spinal cords were subjected to double staining of GFP (green) with HuC/D (***C***, ***F***), TuJ1 (***D***), MAP2 (***E***), GFAP (***G***), and GalC (***H***). Arrows indicate double stained cells. In ***C–E***, cell nuclei were stained with DAPI (blue). ***F***, A set of three-dimensional confocal images of a GFP $^+$/HuC/D $^+$ cell. ***I***, Induction of neuronal differentiation of GFP $^+$ cells *in vivo* by GFs. Dissociated cells were prepared from spinal cords treated with (filled bars) and without (open bars) GFs at DAI3 (left) and DAI7 (right), and the percentages of GFP $^+$ cells expressing respective neuronal and glial markers were quantified (mean ± SD; $n = 3–6$ animals) $^*p < 0.01$ compared with untreated animals. Scale bars: (in ***E***) ***A***, ***C–E***, 50 μm; ***B*** and three-dimensional images in ***A***, 20 μm; (in ***G***, ***H***) ***F***, ***G***, ***H***, 10 μm.

dissociated single cells. We found that GFP $^+$ cells contained all three neural cell lineages, and that the percentages of neurons and glia were essentially identical between GFP $^+$ and GFP $^-$ cell populations (Fig. 3*J*). Altogether, these results demonstrate that a fraction of GFP-labeled, virus-infected cells indeed exhibited the properties of NPCs.

Induction of new neurons by growth factors

We next examined differentiation of retrovirus-infected cells *in vivo*. Without administration of GFs, no GFP $^+$ cells expressing neuronal markers were detectable at any time point examined (Fig. 4*I*) (data not shown), indicating that viruses did not infect pre-existing postmitotic neurons. In contrast, we found that in GF-treated spinal cords, a significant fraction of GFP $^+$ cells expressed the immature neuronal markers HuC/D, TuJ1, and c subunit of MAP2 at DAI3 and DAI7 (Fig. 4*A*,*B*,*I*). The costaining of GFP and these markers in the same cells was confirmed under confocal microscope (Fig. 4*A*,*B*, bottom right). Such cells were detected in both the gray and white matters, and their distribution pattern varied among sections examined. The size (9–14 μm in diameter) and shape (round, oval, or spindle) of their soma were also variable at different locations. Yet, they commonly harbored multiple thin processes, typical of differentiating immature neurons. None of these GFP $^+$/neuronal marker-positive cells, however, coexpressed NeuN, a marker commonly used to identify mature neurons (see below). Given the fact that the vast majority of neurons in the adult spinal cord are NeuN $^+$, these results reinforce the idea that GFP viruses did not infect pre-existing neurons.

To further validate the coexpression of neuronal markers and GFP in single cells, GF-treated tissue was dissociated into single cells and seeded on poly-D-lysine-coated dishes. GFP $^+$/neuronal marker-positive cells immediately attached to the culture surface and actively extended processes within 2 h after plating (Fig. 4*C–F*). Thus, they were indeed live neurons, not dead or dying cells. None of these cells harbored multiple or abnormally enlarged nuclei; hence, it is unlikely that fusion between non-neuronal cells and pre-existing neurons, which is known to occur at an extremely low but yet detectable rate in injured adult tissue (Alvarez-Dolado et al., 2003), accounted for the emergence of GFP $^+$/neuronal marker-positive cells. Moreover, when BrdU was coadministered with GFs between DAI0 and DAI2, a small number of BrdU $^+$/TuJ1 $^+$ cells (four cells among total 1090 BrdU $^+$ cells examined; 0.37%) were detected at DAI7, although such cells were never detected in GF-untreated animals (data not shown) (Yamamoto et al., 2001a,b). Thus, the results using both BrdU and GFP viruses supported the idea that new neurons were generated from endogenous cells in GF-treated spinal cords. It has been shown that the expression of various GFs including FGF2 is upregulated after injury (Mocchetti et al., 1996;

Nakamura and Bregman, 2001; Velardo et al., 2004). Given the observed effect of exogenously administered GFs, however, it appears that their endogenous levels are not sufficient to support neurogenesis in the injured spinal cord. This is in sharp contrast to the situation in other parts of the CNS, where detectable neurogenesis occurs after injury without treatment with exogenous GFs (Arvidsson et al., 2002; Nakatomi et al., 2002; Teramoto et al., 2003).

We next quantitatively assessed the induction of new neurons by GFs. At DAI3, 3.0 ± 0.7% of GFP$^+$ cells (19 positive cells/652 cells examined; $n = 3$ animals) were TuJ1$^+$, and this percentage increased to 22.8 ± 1.9% at DAI7 (224 cells/995 GFP$^+$ cells examined; $n = 4$ animals) (Fig. 4*I*). At DAI7, 28.9 ± 6.2 and 4.2 ± 1.4% of GFP$^+$ cells were also HuC/D$^+$ and MAP2$^+$, respectively. The percentage of GFP$^+$/HuC/D$^+$ cells in animals treated with a lower dose of GFs was much smaller (<5%), suggesting a dose-dependent effect of GFs on neuronal differentiation. Given that 4.67×10^4 and 4.00×10^4 GFP$^+$ cells were detected at DAI3 and DAI7, respectively, the estimated number of GFP$^+$/TuJ1$^+$ cells was 1.40×10^3 at DAI3 and 9.10×10^3 at DAI7 per GF-treated animal ($n = 3$). Thus, new neurons substantially increased in number between DAI3 and DAI7 ($p < 0.01$), whereas the total number of GFP$^+$ cells rather decreased to 86% during this period. This time-dependent increase in the actual number of GFP$^+$/neuronal marker-positive cells reinforces the idea that such cells were unlikely to be products of cell fusion between pre-existing neurons and non-neuronal cells, or mere artifacts in histology. Furthermore, albeit that GF-treatment increased the number of GFP$^+$ cells only 1.6-fold at DAI3 and 2.7-fold at DAI7, GFP$^+$ cells expressing neuronal markers were not detected at all in untreated animals. These results are consistent with the idea that GFs not only stimulated proliferation of endogenous NPCs, but also promoted their neuronal differentiation *in vivo*. GFs might have supported the survival of newly generated neurons as well, but such a survival effect could not fully account for the observed increase in the number of new neurons between DAI3 and DAI7. We found, however, that the numbers of GFP$^+$/TuJ1$^+$ and GFP$^+$/HuC/D$^+$ cells gradually decreased after DAI7, and they eventually disappeared by DAI28 (data not shown). In addition, as described above, no GFP$^+$ cells were found to express NeuN, which features a more mature phenotype of neurons, at any time points examined when control viruses were used for infection (see below).

Unlike these neuronal cells, substantial fractions of GFP$^+$ cells expressed glial cell markers GFAP (Fig. 4*G*) and GalC (Fig. 4*H*) without treatment with GFs, and their percentages were not significantly different between GF-treated and untreated animals ($p = 0.160$ for GFAP$^+$ cells and $p = 0.327$ for GalC$^+$ cells) (Fig. 4*I*). Few GFP$^+$ or BrdU$^+$ cells were GalC$^+$ at earlier time points, suggesting that GFP$^+$/GalC$^+$ cells detected at DAI7 were newly generated oligodendrocytes. In fact, it has been demonstrated that immature oligodendrocytes are generated in both the intact and injured spinal cord (McTigue et al., 1998, 2001; Horner et al., 2000; Ishii et al., 2001; Watanabe et al., 2002, 2004; Talbott et al., 2005; Yang et al., 2006). Nevertheless, we detected no GFP$^+$ cells expressing MBP or PLP, markers for myelin-forming oligodendrocytes, at any time points examined in either GF-treated or untreated animals. Thus, the maturation of oligodendrocytes appeared to be limited in injured tissue (see below). Unlike these cells in the oligodendrocyte lineage, many GFP$^+$/GFAP$^+$ and BrdU$^+$/GFAP$^+$ astrocytes were detected at both DAI3 and DAI7 (Figs. 1*I*, 4*I*). Because mature astrocytes are known to retain the ability of cell divisions, it remained undetermined to what extent GFP$^+$/GFAP$^+$ cells reflected *de novo* differentiation of NPCs into the astrocyte lineage.

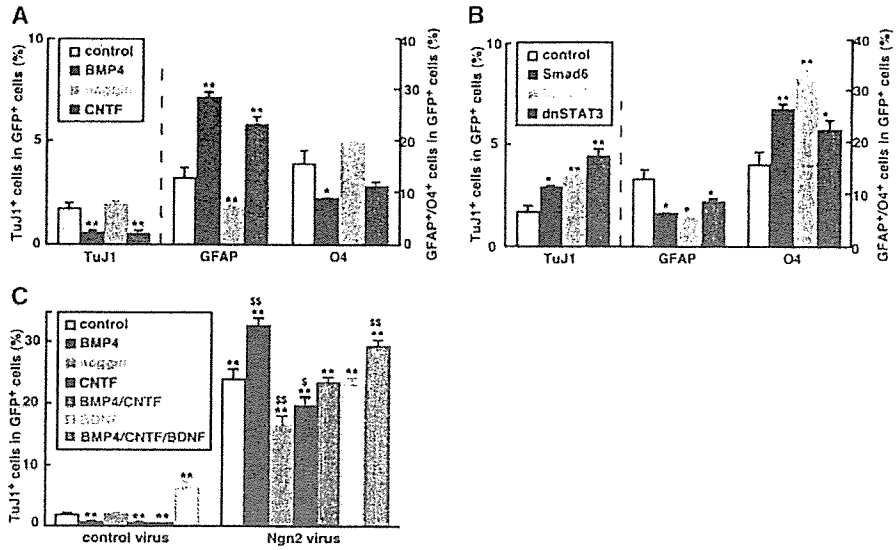

Figure 5. Manipulation of neuronal differentiation of NPCs by Ngn2 *in vitro*. *A*, Neuronal and glial differentiation of GFP virus-infected neurosphere cells in the presence of various extracellular factors. Percentages of TuJ1$^+$, GFAP$^+$, and O4$^+$ cells among total GFP$^+$ cells treated with BMP4 (blue bars), noggin (green bars), and CNTF (red bars) are compared with those of untreated control cells (open bars). *B*, Effects of blocking BMP and CNTF signaling. Neurosphere-forming NPCs were infected with retroviruses overexpressing Smad6 (blue bars), Smad7 (green bars), and dn-STAT3 (red bars), and their differentiation patterns were compared with that of control virus-infected cells (open bars). *C*, Effect of Ngn2 on neuronal differentiation of NPCs. Neurosphere-forming NPCs were infected with retroviruses overexpressing Ngn2 (right), and their neuronal differentiation in the presence of various extracellular factors (BMP4, blue bars; noggin, light green bars; CNTF, red bars; BMP4 plus CNTF, dark green bars; BDNF, yellow bars; BMP4 plus CNTF plus BDNF, orange bars) were compared with that of control virus-infected cells (left). All data in *A–C* are mean ± SD (3–5 independent culture experiments; $^*p < 0.05$ and $^{**}p < 0.01$ compared with the control; $^{\$}p < 0.05$ and $^{\$\$}p < 0.01$ compared with Ngn2 alone).

Enhanced neurogenesis by Neurogenin2 and BDNF *in vitro*

The above study demonstrated that the production of new neurons from endogenous NPCs can be induced under certain conditions. This, in turn, suggests the presence of certain mechanisms that actively suppress the neurogenic potential of NPCs *in situ*. We first addressed this issue using *in vitro* culture of NPCs. To mimic the situation of virus-infected NPCs *in vivo*, growing neurosphere cells were infected with pMXIG viruses, and subsequently, neuronal and glial differentiation of GFP$^+$ cells after removal of GFs was examined (Fig. 5).

It has been shown that the expression of various cytokines is significantly upregulated in the injured spinal cord (Nakamura and Bregman, 2001; Setoguchi et al., 2001, 2004; Velardo et al., 2004; Chen et al., 2005). Among them, BMPs and CNTF have been shown to inhibit neuronal differentiation of NPCs both *in vivo* and *in vitro* (Lim et al., 2000; Nakashima et al., 2001; Setoguchi et al., 2004). Consistent with this, treatment of neurospheres with BMP4 and CNTF significantly increased the percentage of

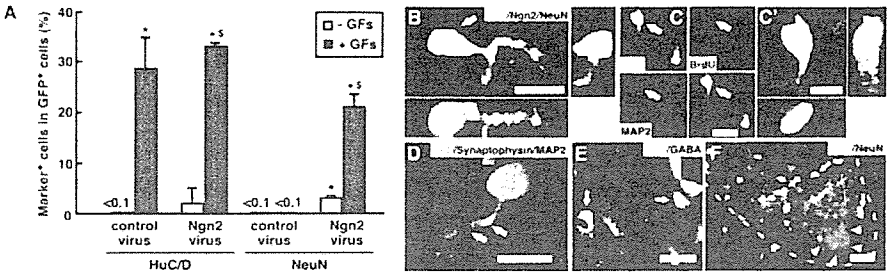

Figure 6. Induction of new neurons by GFs, Ngn2, and BDNF *in vivo*. ***A***, Effects of GFs and Ngn2 on neuronal differentiation of GFP-labeled cells *in vivo*. Control and Ngn2 viruses were administered with (red bars) or without (white bars) GFs into injured spinal cords, and subsequently the percentages of HuC/D$^+$ (left) and NeuN$^+$ (right) cells among total GFP$^+$ cells were quantified at DAI7. GFP$^+$/HuC/D$^+$ cells were detected in dissociated single cells, whereas GFP$^+$/NeuN$^+$ cells were detected in tissue sections. $^*p < 0.01$ compared with control virus-infected animals. $^\$p < 0.01$ compared with Ngn2 without GFs. ***B–F***, Micrographs showing GFP$^+$ cells (green) costained for Ngn2 (red) and NeuN (blue) (***B***) and BrdU (red) and MAP2 (blue) (***C***, ***C'***) at DAI7, synaptophysin (red) and MAP2 (blue) (***D***), GABA (red) (***E***), and NeuN (red) (***F***) at DAI28. ***C'*** shows a magnified view of a neurons indicated by arrow in ***C***. The right and bottom panels in ***B*** and ***C'*** show three-dimensional digital images of cells triple positive for respective markers. Note that the overlap of green, red, and blue colors in single cells results in white color. Arrows in ***D*** indicate synaptophysin$^+$ dense speckles associated with processes of GFP$^+$/MAP2$^+$ cells. Arrows in ***E*** and ***F*** indicate GFP$^+$/GABA$^+$ and GFP$^+$/NeuN$^+$ cells, respectively. A dashed line in ***F*** demarcates the position of the anterior horn where GFP$^+$/NeuN$^+$ small interneuron-like cells intermingled with large motoneurons (indicated by arrowheads). Scale bars: ***B***, ***C'***, 10 μm; ***C***, ***D***, ***E***, 20 μm; ***F***, 50 μm.

GFAP$^+$ astrocytes among total GFP$^+$ cells, and this occurred at the expense of TuJ1$^+$ neurons and O4$^+$ oligodendrocytes ($p < 0.001$ for both BMP4 and CNTF) (Fig. 5*A*). These factors did not significantly alter the rate of cell proliferation or death of either GFP$^+$ or GFP$^-$ cells in culture (data not shown) and, thus, the observed effects most likely reflected their actions on differentiation of NPCs. Conversely, the extracellular BMP inhibitor noggin decreased the fraction of GFAP$^+$ cells (Fig. 5*A*). Retrovirus-mediated overexpression of Smad6 and Smad7, which block intracellular signaling for BMP4, also exerted the same effect (Fig. 5*B*). Likewise, a dominant-negative (dn) form of STAT3 (Kamakura et al., 2004), which inhibits the activity of endogenous STAT3, the major intracellular signal transducer downstream of CNTF receptors (Sun et al., 2001; Kamakura et al., 2004), increased the percentages of TuJ1$^+$ and O4$^+$ cells ($p < 0.001$ for TuJ1 and $p < 0.01$ for O4) (Fig. 5*B*). These results suggest that BMP4 and CNTF (or related cytokines) are expressed by NPCs themselves and/or their progeny, and that such endogenous factors inhibit neurogenesis in an autocrine and/or paracrine manner. This could be one of the mechanisms by which neuronal differentiation of NPCs is attenuated *in vivo*. However, the effect of blocking the actions of these endogenous cytokines on neurogenesis was rather weak: <5% of total GFP$^+$ cells differentiated into neurons under the conditions in which cytokine signals were attenuated by Smad6/7, dn-STAT3, or both (Fig. 5*B*) (data not shown). Furthermore, the stimulatory effect of noggin on neuronal differentiation of NPCs appears to be variable *in vivo* (Setoguchi et al., 2004; Enzmann et al., 2005).

We therefore tested another strategy to enhance neurogenesis by NPCs. Our previous study suggested that signaling through the cell-surface receptor Notch is involved in the inhibition of neuronal differentiation of NPCs, and that overexpression of the neurogenic transcription factor Ngn2 can overcome such inhibition (Yamamoto et al., 2001b). A more recent study has also shown that Ngn2 enhances neuronal differentiation of grafted, exogenous NPCs *in vivo* (Hofstetter et al., 2005). Then, we tested whether Ngn2 can also stimulate neurogenesis in the presence of BMP4 and CNTF *in vitro*. When neurospheres were infected with Ngn2-expressing retroviruses, 23.9 ± 1.7% of total GFP$^+$ cells became TuJ1$^+$ compared with 1.7 ± 0.3% in the control culture ($p < 0.0001$; $n = 3$) (Fig. 5*C*). Under the same conditions, the percentages of GFAP$^+$ astrocytes and O4$^+$ oligodendrocytes were not significantly different between control and Ngn2 virus-infected cells (data not shown) (Yamamoto et al., 2001b). Importantly, the neurogenic action of Ngn2 was preserved in the presence of exogenous BMP4 and CNTF. Even a higher percentage of Ngn2-expressing NPCs differentiated into neurons in the presence of BMP4 than in its absence ($p < 0.001$), consistent with a previous study using embryonic brain-derived NPCs (Sun et al., 2001). Moreover, BDNF, which promotes differentiation and survival of new neurons in the adult CNS (Namiki et al., 2000; Coumans et al., 2001; Chmielnicki et al., 2004), increased the percentage of TuJ1$^+$ neurons generated by Ngn2-expressing cells (29.4 ± 1.0%; $n = 3$; $p < 0.005$).

Stimulation of neurogenesis by Ngn2 and BDNF *in vivo*

Based on these *in vitro* results, we next tested the activities of Ngn2 viruses and BDNF *in vivo*. Unlike control virus-infected cells, a small, but significant percentage of Ngn2 virus-infected cells became HuC/D$^+$ (2.3 ± 3.2%; $n = 3$) and NeuN$^+$ (3.0 ± 0.1; $n = 3$) at DAI7 even without cotreatment with GFs (Fig. 6*A*). Furthermore, when combined with GFs, much larger fractions of Ngn2-expressing cells become HuC/D$^+$ and NeuN$^+$ (33.3 ± 0.6 and 21.1 ± 2.3%, respectively; $n = 3$ animals; $p < 0.01$). In the presence of GFs, however, the percentages of GFP$^+$/HuC/D$^+$ cells did not significantly differ between control and Ngn2 virus-infected animals ($p = 0.1404$). Thus, GF treatment appeared to exert a stronger effect than Ngn2 overexpression on the generation of HuC/D$^+$ immature neurons *in vivo*. Yet, the combination of Ngn2 and GFs showed a much stronger activity to induce GFP$^+$/NeuN$^+$ cells compared with those of GFs and Ngn2 alone ($p < 0.01$), suggesting that these two manipulations collaborate to induce NeuN$^+$ neurons.

The coexpression of Ngn2 confirmed that GFP$^+$/NeuN$^+$ neurons were derived from Ngn2 virus-infected cells (Fig. 6*B*). Moreover, many GFP$^+$/NeuN$^+$ cells were also labeled with BrdU administered between DAI0 and DAI2, indicating that such cells were indeed generated by cells that proliferated *in situ* (Fig. 6*C*). Under our experimental conditions, control and Ngn2 viruses are thought to infect the same cells population *in situ* with or without GFs. Nevertheless, GFP$^+$/NeuN$^+$ cells were detected only in Ngn2 virus-infected animals. Thus, we conclude that the possibility that the costaining of GFP and NeuN was caused by certain artifacts is highly unlikely.

As shown in Figure 6, *C* and *D*, many GFP$^+$ cells in Ngn2 virus-infected tissues developed thick processes with intense MAP2 staining. Their soma and processes were often associated with synaptophysin$^+$ dense speckles reminiscent of synaptic buttons of surrounding preexisting neurons (Fig. 6*D*, arrows), suggesting more mature properties of GFP$^+$/NeuN$^+$ neurons than those of GFP$^+$/HuC/D$^+$ cells. Most (>95%) of these GFP$^+$/NeuN$^+$ neurons were positive for GABA (Fig. 6*E*), but negative for choline acetyltransferase or glycine (data not shown), suggesting that they differentiated into certain types of interneurons. For

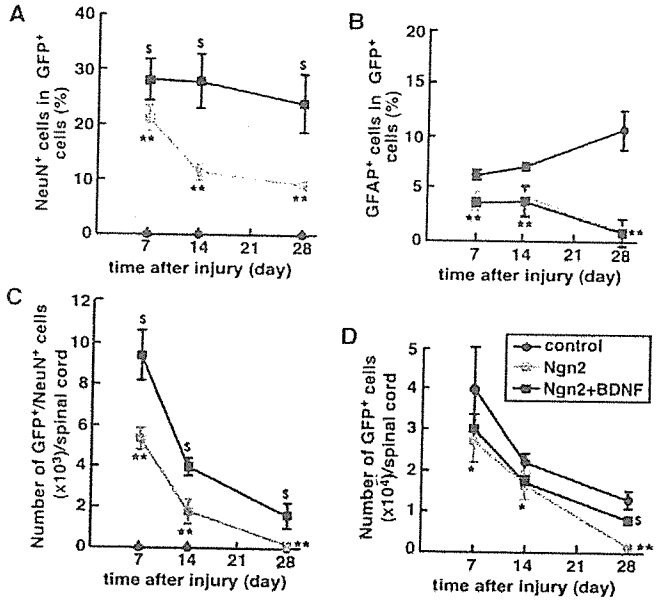

Figure 7. Survival of newly generated neurons in injured spinal cords. ***A–D***, Percentages of NeuN$^+$ (*A*) and GFAP$^+$ (*B*) cells among total GFP$^+$ cells, and estimated numbers of GFP$^+$/NeuN$^+$ (*C*) and total GFP$^+$ (*D*) cells were quantified at various time points after injury. Injured spinal cords were treated with GFs and control viruses (red lines), GFs and Ngn2 viruses (green), and GFs, BDNF, and Ngn2 viruses (blue). All data are mean ± SD (3–12 independent experiments; $^*p < 0.05$ and $^{**}p < 0.01$ compared with control virus infection; $^{\$}p < 0.01$ compared with Ngn2 virus infection alone).

example, GFP$^+$/NeuN$^+$ cells detected in the anterior horn were scattered within a cluster of large motor neurons and smaller interneurons, but their soma size (10–19 μm in diameter; 14.4 ± 3.3 μm; $n = 6$) was similar to that of the latter subtype (14.5 ± 3.7 μm; $n = 8$) (Fig. 6*F*). However, the morphology and location of individual GFP$^+$/NeuN$^+$ cells were highly variable depending on their relative distance from the lesion epicenter and also among treated animals. Moreover, none of these neurons expressed subtype-specific molecular markers examined such as HB9, Islet1, Lim1, and Lim3 (Yamamoto et al., 2001b and references therein), and therefore whether they differentiated into specific neuronal subtypes remained undetermined.

The coadministration of BDNF with GFs neither increased the percentage of GFP$^+$/HuC/D$^+$ cells compared with GF treatment alone, nor induced GFP$^+$/NeuN$^+$ cells in control virus-infected animals (no GFP$^+$/NeuN$^+$ cells among 652 GFP$^+$ cells examined). When combined with Ngn2 and GFs, however, BDNF significantly increased the percentage of GFP$^+$/NeuN$^+$ cells among total GFP$^+$ cells (28.2 ± 3.4%; $n = 3$ animals; $p < 0.01$ compared with animals without BDNF treatment) (Fig. 7*A*). Concomitant with this increase, the percentage of GFP$^+$/GFAP$^+$ cells was significantly lower in both Ngn2/GF- and Ngn2/GF/BDNF-treated animals compared with the control level (3.8 ± 0.9 and 3.7 ± 0.4% vs 6.3 ± 0.5%; $p < 0.01$) (Fig. 7*B*). This decrease alone, however, could not fully account for the much larger increase of GFP$^+$/NeuN$^+$ cells, suggesting that Ngn2 and BDNF did not simply inhibit gliogenesis, but rather actively promoted generation of neurons.

We further followed the survival of GFP$^+$/NeuN$^+$ cells *in vivo*. At DAI7, the estimated number of GFP$^+$/NeuN$^+$ neurons was 5.4 ± 0.5 × 10^3 ($n = 3$) per spinal cord in Ngn2 virus-infected/GF-treated animals (Fig. 7*C*). Their numbers, however, were only 33 and 3% at DAI14 and DAI28, respectively, compared with that detected at DAI7. Although the total number of GFP$^+$ cells decreased during this period (Fig. 7*D*), the percentage of NeuN$^+$ neurons among them also decreased over time (Fig. 7*A*). Thus, GFP$^+$/NeuN$^+$ new neurons appeared to be eliminated faster than other GFP$^+$ cell populations in injured tissue. Silencing of the GFP transgene could partly explain the observed loss of GFP-labeled new neurons (Vroemen et al., 2003). However, a higher percentage (33%) of control virus-infected cells, in which the fraction of new neurons was much smaller, survived up to DAI28. Furthermore, we observed longer survival of Ngn2 virus-infected cells in other parts of the CNS (our unpublished results). Thus, we favor the idea that the observed decrease reflected the actual loss of new neurons in injured spinal cords. Consistent with this idea, when the neurotrophic factor BDNF, which is thought to promote survival of neurons, increased the number of GFP$^+$/NeuN$^+$ cells 1.9-fold in Ngn2/GF-treated animals at DAI7 (9.4 ± 0.2 × 10^3; $n = 4$; $p < 0.001$ in two-tailed unpaired *t* test) (Fig. 7*C*). Moreover, larger numbers of GFP$^+$/NeuN$^+$ cells remained at DAI14 and DAI28 in BDNF-treated animals ($p < 0.0001$) (Fig. 7*C*). However, few GFP$^+$/NeuN$^+$ cells remained detectable at DAI56 or later time points (data not shown). Thus, the long-term survival of newly generated neurons appears to be very limited in the injured spinal cord.

Stimulation of oligodendrogenesis by Mash1

We next tested the effect of another proneural transcription factor, Mash1, which has been implicated in both neurogenesis and oligodendrogenesis during development (Parras et al., 2004). When NPCs were isolated as neurospheres from Mash1 virus-infected tissue, significantly higher percentages of Mash1-expressing cells differentiated into O4$^+$ and GalC$^+$ oligodendrocytes, and conversely, a much smaller fraction became GFAP$^+$ astrocytes compared with control virus-infected cells (Fig. 8*A*). Unlike Ngn2, Mash1 did not change the percentage of TuJ1$^+$ neurons among GFP$^+$ cells. Thus, Mash1 selectively increased oligodendrocytes in culture of adult spinal cord NPCs.

As described above, a substantial fraction of control virus-infected cells were GalC$^+$ *in vivo* (Fig. 4*I*). These results are consistent with previous studies in which production of new oligodendrocytes by NG2$^+$ cells was detected under various insult conditions (McTigue et al., 1998, 2001; Ishii et al., 2001; Watanabe et al., 2002, 2004; Talbott et al., 2005; Zai and Wrathall, 2005; Yang et al., 2006). In line with this, we found that some NG2$^+$ cells in injured tissue expressed endogenous Mash1 (Fig. 8*B*). This is in sharp contrast to endogenous Ngn2; we could not detect any cells expressing Ngn2 at any time point examined after injury (data not shown) (Yamamoto et al., 2001b). Such NG2$^+$/Mash1$^+$ cells, however, were small in number at DAI14, and almost disappeared at DAI28. These results raise the possibility that endogenous Mash1 is involved in the generation of new oligodendrocytes, but its limited expression accounts for their restricted generation and maturation in injured tissue.

To test this idea, we examined the effect of constitutive overexpression of Mash1 together with GF treatment *in vivo*. Consistent with the results of the above *in vitro* experiments, significantly larger fractions of Mash1 virus-infected cells became GalC$^+$ and GST-π$^+$ oligodendrocytes compared with control virus-infected cells (Fig. 8*C*,*F*). Over one-third (38.9 ± 7.2%; $n = 4$ animals) of total Mash1-expressing cells were GST-π$^+$ at DAI7 (Fig. 8*F*). Because few GFP$^+$ cells expressed these markers at DAI3, these results suggest that Mash1 stimulated the production of new oligodendrocytes *in situ*. Furthermore, at DAI28, a small but significant fraction of GFP$^+$ cells expressed RIP (Fig. 8*D*) and PLP (Fig. 8*E*), markers for more mature, myelin-forming